ministerie van verkeer en waterstaat

**koninklijk nederlands meteorologisch instituut**

# a baroclinic two-layer ocean model on an equatorial β-plane

AJM Verhaar

technische rapporten TR-82

technical reports TR-82

KNMI

Contents

ABSTRACT

This is a technical report about a baroclinic two-layer ocean model. The basic idea has been taken from Anderson and McCreary (1985). It is an extension of the usual reduced-gravity model in that active thermodynamics is included and will be used in experiments with coupled equatorial ocean-atmosphere models.

We also present some examples of its first-stage performance. Results of these experiments show satisfactory agreement with theory.

# 1. THE MODEL

## 1.1 Introduction

The vertical density structure of the equatorial ocean consists generally of a well-mixed surface layer of constant density above a sharp pycnocline. A typical value of the mixed layer thickness is 100-200 m.
A prominent feature of the pycnocline is that it can move vertically a considerable distance in relatively short periods of time. The simplest models capable of simulating this behaviour are reduced-gravity models. They assume the ocean to consist of a thin surface layer of density $\rho$ overlying an infinitely deep lower layer of density $\rho + \Delta\rho$ and they describe variations of the mixed layer thickness.

Another feature of the equatorial ocean is the occurrence of large and persistent sea surface temperature (SST) anomalies (e.g. as during an ENSO-event). Since ordinary reduced-gravity models do not treat the temperature of the upper layer as a variable, a thermodynamic equation is required to include the evolution of SST-anomalies.
In this extended reduced-gravity model we also allow for mass and energy exchange between the layers by various processes. The exchange processes are added in parameterized form to the thermodynamic and continuity equation.

In the first few experiments described in this report the effects of thermodynamics and the parameterized exchange processes between the two layers have been neglected.

## 1.2 Model assumptions and equations

The model equations are derived from the shallow-water equations on an equatorial $\beta$-plane, including horizontal stress and eddy viscosity:

$$\frac{\partial \vec{u}}{\partial t} + \vec{u}.\nabla\vec{u} + \beta y\vec{k} \times \vec{u} = -\frac{1}{\rho}\nabla p + \frac{1}{\rho}\frac{\partial \vec{\tau}}{\partial z} + \nu\nabla^2\vec{u} \qquad (1.1)$$

$$\frac{\partial h}{\partial t} + \nabla.(h\vec{u}) = 0 \qquad (1.2)$$

$$\frac{\partial p}{\partial z} = -\rho g \qquad (1.3)$$

in which $\vec{x}$ is the horizontal stress vector and $\nu$ the eddy coefficient of viscosity. All other symbols have their usual meaning.
Figure 1 shows a vertical cross-section of a two-layer ocean. Layer 1 (the mixed layer) has variable density and temperature $\rho_1$ and $T_1$ respectively. The underlying, much deeper, layer 2 has a slightly greater density $\rho_2$ and temperature $T_2$, which are both constant. Neglecting effects of salinity and compressibility, the density ratio of the two layers is a function of $T \equiv T_1 - T_2$ only. We use:

$$\rho_1 = \rho_2(1-\alpha T) \tag{1.4}$$

with $\alpha$ the thermal expansion coefficient.
It can be seen from the Figure:

$$h_1 = H_1 + \eta_1 - \eta_2 \tag{1.5}$$

$$h_2 = H_2 + \eta_2 \tag{1.6}$$

$$H = H_1 + H_2 \tag{1.7}$$

With the appropriate indices eqs. (1.1)-(1.3) can be applied to both layer 1 and 2.
Expressions for $p_1$ and $p_2$ follow from the application of the hydrostatic equation:

$$p_1 = \rho_1 g (\eta_1 - z) \tag{1.8}$$

$$p_2 = \rho_1 g h_1 + \rho_2 g (- H_1 + \eta_2 - z) \tag{1.9}$$

Having two degrees of freedom, the two-layer system allows two normal modes of motion: the barotropic and the baroclinic mode. Since we will be concerned with the latter (slow) mode only, the barotropic mode will be eliminated. For the baroclinic mode it can be shown that (see Gill (1982, pp. 119-128)):

$$\frac{\|\vec{u}_2\|}{\|\vec{u}_1\|} \approx \frac{H_1}{H_2} \tag{1.10}$$

Taking the limit $H_2 \to \infty$ it is seen that $\vec{u}_2 \to \vec{0}$. Consequently no pressure gradient exists in the lower layer, i.e.

$$\lim_{H_2 \to \infty} \frac{1}{\rho_2} \nabla p_2 = \vec{0} \tag{1.11}$$

Substituting (1.9) for $p_2$ and using (1.4) and (1.5) it follows that

$$\nabla \eta_1 = \alpha \nabla (h_1 T) \tag{1.12}$$

This equation shows how the effect of a sloping free surface can be compensated for, in order that the pressure gradient in the lower layer vanish. Two special cases are depicted in Figure 2.
An expression for the upper layer pressure gradient is found using (1.8). Substituting (1.12) for $\nabla \eta_1$ and using the Boussinesq approximation (here $\frac{\rho 2}{\rho 1} \approx 1$) it follows that

$$-\frac{1}{\rho_1} \nabla p_1 = -\alpha g \nabla(h_1 T) + \alpha g (\eta_1 - z) \nabla T \tag{1.13}$$

$\eta_1$ is eliminated from this equation by vertical integration over the upper layer:

$$\int_{-H_1+\eta_2}^{\eta_1} -\frac{1}{\rho_1} \nabla p_1 \, dz = -\tfrac{1}{2} \alpha g \nabla (h_1^2 T) \tag{1.14}$$

Horizontal stress $\vec{x}$ is assumed to be non-zero in the upper layer only and to satisfy the following boundary conditions:

$$\vec{x} = \vec{\tau} \text{ at the free surface} \tag{1.15}$$

in which $\vec{\tau} = (\tau_x, \tau_y)$ represents the surface wind stress vector and

$$\vec{x} = \vec{0} \text{ at the interface} \tag{1.16}$$

Assuming $\vec{x}$ to be a linear function of z in the upper layer, $\vec{u}_1$ can consistently be considered independent of z. Integration of the momentum equation (1.1) over layer 1 (index 1) then yields, using (1.14)-(1.16):

$$h_1 \frac{\partial \vec{u}_1}{\partial t} + h_1 \vec{u}_1 \cdot \nabla \vec{u}_1 + \beta h_1 y \vec{k} \times \vec{u}_1 = -\tfrac{1}{2} \alpha g \nabla (h_1^2 T) + \frac{\vec{\tau}}{\rho_1} + \nu h_1 \nabla^2 \vec{u}_1 \tag{1.17}$$

This equation can also be written in the flux form. The scalar components of this form read:

$$\frac{\partial hu}{\partial t} + \frac{\partial huu}{\partial x} + \frac{\partial huv}{\partial y} - \beta yhv = -\tfrac{1}{2}\alpha g \frac{\partial}{\partial x}(h^2T) + \frac{\tau_x}{\rho_o} + \nu h\nabla^2 u \qquad (1.18)$$

$$\frac{\partial hv}{\partial t} + \frac{\partial hvu}{\partial x} + \frac{\partial hvv}{\partial y} + \beta yhu = -\tfrac{1}{2}\alpha g \frac{\partial}{\partial y}(h^2T) + \frac{\tau_y}{\rho_o} + \nu h\nabla^2 v \qquad (1.19)$$

in which the index 1 is ignored for notational simplicity and $\rho_0 \equiv \rho_2 \approx \rho_1$.

As $T_1$ is allowed to be a function of position and time a thermodynamic equation is needed to close the system of equations. The exchange processes referred to in section 1.1 enter this equation and the equation of continuity (1.2) for layer 1 in parameterized form. In formula:

$$\frac{\partial h_1}{\partial t} + \frac{\partial h_1 u_1}{\partial x} + \frac{\partial h_1 v_1}{\partial y} = R_I\,(h_1, T_1, T_2) \qquad (1.20)$$

$$\frac{\partial T_1}{\partial t} + u_1 \frac{\partial T_1}{\partial x} + v_1 \frac{\partial T_1}{\partial y} = R_{II}^{*}\,(h_1, T_1, T_2) + \kappa \nabla^2 T_1 \qquad (1.21)$$

The terms $R_I$ and $R_{II}^{*}$ describe the effects of entrainment by turbulent mixing and an external heat source. An example can be found in Anderson and McCreary (1985). The last term at the RHS of (1.21) represents the diffusive effects of eddies.

Replacing $T_1$ by T in (1.21) in the terms involving derivatives of $T_1$ ($T_2$ is constant) and again ignoring the layer index 1 elsewhere, equations (1.20) and (1.21) become:

$$\frac{\partial h}{\partial t} + \frac{\partial hu}{\partial x} + \frac{\partial hv}{\partial y} = R_I \qquad (1.22)$$

$$\frac{\partial hT}{\partial t} + \frac{\partial huT}{\partial x} + \frac{\partial hvT}{\partial y} = R_{II} + \kappa h\nabla^2 T \qquad (1.23)$$

the latter written in the flux form.

## 1.3 Energetics and integral constraints

Using the rigid lid approximation ($\eta_1 = 0$) for the baroclinic mode, (1.5) becomes, ignoring the layer index 1 at the LHS:

$$h = H_1 - \eta_2 \qquad (1.24)$$

The kinetic energy per horizontal unit area for the upper layer is given by:

$$K_1 = \int_{-H_1+\eta_2}^{0} \tfrac{1}{2} \rho \vec{u}^2 \, dz = \tfrac{1}{2} \rho_1 \vec{u}_1^2 (H_1 - \eta_2)$$

Similarly for the lower layer:

$$K_2 = \int_{-H}^{-H_1+\eta_2} \tfrac{1}{2} \rho \vec{u}^2 \, dz = \tfrac{1}{2} \rho_2 \vec{u}_2^2 (H - H_1 + \eta_2)$$

With (1.10) it follows that for $H_2 > H_1$, $K_2 < K_1$.
The total kinetic energy is then approximately given by, using (1.24),

$$K = \tfrac{1}{2} \rho_0 h \vec{u}^2 \tag{1.25}$$

in which $\vec{u} \equiv \vec{u}_1$ and $\rho_0 \equiv \rho_2 \approx \rho_1$.

For the potential energy per horizontal unit area we find:

$$P_1 = \int_{-H_1+\eta_2}^{0} \rho g z \, dz = - \tfrac{1}{2} \rho_1 g h^2$$

$$P_2 = \int_{-H}^{-H_1+\eta_2} \rho g z \, dz = \tfrac{1}{2} \rho_2 g [h^2 - H^2]$$

in which (1.24) has been used.
The total potential energy, after use of (1.4) is:

$$P = - \tfrac{1}{2} \rho_2 g H^2 + \tfrac{1}{2} \rho_2 \alpha T g h^2$$

or, ignoring the first, constant, term and $\rho_0 \equiv \rho_2$:

$$P = \tfrac{1}{2} \rho_0 \alpha T g h^2 \tag{1.26}$$

Finally, the enthalpy per horizontal unit area of layer 1 is given by:

$$E = \rho_0 c_p h T_1 \tag{1.27}$$

Integral constraints for a closed basin are derived from the inviscid, unforced and non-diffusive forms of equations (1.18), (1.19), (1.22) and (1.23).

Multyplying (1.18) by u, (1.19) by v, (1.22) by $u^2 + v^2$ and adding the results yields the kinetic energy equation:

$$\frac{\partial}{\partial t}\left(\tfrac{1}{2} h \vec{u}^2\right) + \nabla \cdot \left(\vec{u}\, \tfrac{1}{2} h \vec{u}^2\right) + \tfrac{1}{2} \alpha g \vec{u} \cdot \nabla (h^2 T) = 0 \qquad (1.28)$$

An equation for the potential energy, defined by (1.26), is found by suitable manipulation of (1.22) and (1.23):

$$\frac{\partial}{\partial t}\left(\tfrac{1}{2} \alpha g h^2 T\right) + 2\nabla \cdot \left(\vec{u}\, \tfrac{1}{2} \alpha g h^2 T\right) - \tfrac{1}{2} \alpha g \vec{u} \cdot \nabla (h^2 T) = 0 \qquad (1.29)$$

The Coriolis force makes no contribution to the rate of change of kinetic energy. The sum of the last terms at the LHS of (1.28) and (1.29) is identically zero, indicating that these are both conversion terms.
Now consider any closed region S with $\vec{u} \cdot \vec{n} = 0$ everywhere at the boundaries ($\vec{n}$ outward unit normal vector), implying rigid, impermeable boundaries.
If the sum of (1.28) and (1.29) is integrated over the interior of S, it is found that the mechanical energy within S is a conserved quantity. Integration of (1.22) yields the statement of mass conservation. With little more effort, recalling $T = T_1 - T_2$ and definition (1.27) for the enthalpy E, the area-integrated form of (1.23) can be recognized as the statement of conservation of enthalpy.

# 2. THE NUMERICAL MODEL

## 2.1 Introduction

The numerical model is a finite difference model with the equations discretized on an Arakawa-C grid.

Space differencing will be such that the integral constraints of section 1.3, derived for a continuous medium, are satisfied in their discrete form. This is of particular importance because of the long-term integrations to be performed with the model. The basis for the present finite difference scheme has been taken from Haltiner and Williams (1979) which itself is a simplified form of a more general scheme proposed by Arakawa and Lamb (1977). The latter scheme is designed to conserve both energy and enstrophy for non-divergent flow.

## 2.2 Space differencing: fluxes, pressure gradient and Coriolis terms

The Arakawa-C grid is shown in Figure 3, with T defined at h-points. The grid size is denoted by d.

For notational simplicity we define:

$$(\overline{A}^{x})_{i,j} \equiv \tfrac{1}{2}(A_{i+\frac{1}{2},j} + A_{i-\frac{1}{2},j}) \tag{2.1}$$

$$(\delta_x A)_{i,j} \equiv A_{i+\frac{1}{2},j} - A_{i-\frac{1}{2},j} \tag{2.2}$$

in which i and j are grid point indices in the x and y directions, respectively. The symbols $(\overline{A}^{y})_{i,j}$ and $(\delta_y A)_{i,j}$ are defined in a similar manner but with respect to the y direction, and

$$(\overline{A}^{xy})_{i,j} \equiv (\overline{\overline{A}^{y}}^{x})_{i,j} \tag{2.3}$$

At h-points the continuity equation (1.22), retaining only the divergence terms, is represented as:

$$\frac{\partial}{\partial t} h_{i,j} + \frac{1}{d^2}[\delta_x F + \delta_y G]_{i,j} = 0 \tag{2.4}$$

with the mass fluxes

$$F_{i+\frac{1}{2},j} \equiv d\,[\overline{h}^{x}u]_{i+\frac{1}{2},j}$$

$$G_{i,j+\frac{1}{2}} \equiv d\,[\overline{h}^{y}v]_{i,j+\frac{1}{2}} \qquad (2.5)$$

defined at u and v points respectively (see Figure 4).

The discrete forms of the momentum equations (1.18) and (1.19) without forcing and viscosity terms are chosen as:

$$\frac{\partial}{\partial t}(\hat{h}^{(u)}u)_{i,j} + \frac{1}{d^2}\left[\delta_x(\hat{F}^{(u)}\,\overline{u}^{x}) + \delta_y(\hat{G}^{(u)}\,\overline{u}^{y})\right]_{i,j}$$
$$-\beta(y\overline{hv}^{xy})_{i,j} + \frac{1}{2d}\alpha g\left[\overline{h}^{x}\delta_x(hT) + \overline{h}^{x}\,\overline{T}^{x}\delta_x h\right]_{i,j} = 0 \qquad (2.6)$$

$$\frac{\partial}{\partial t}(\hat{h}^{(v)}v)_{i,j} + \frac{1}{d^2}\left[\delta_x(\hat{F}^{(v)}\,\overline{v}^{x}) + \delta_y(\hat{G}^{(v)}\,\overline{v}^{y})\right]_{i,j}$$
$$+\beta(y\overline{hu}^{xy})_{i,j} + \frac{1}{2d}\alpha g\left[\overline{h}^{y}\delta_y(hT) + \overline{h}^{y}\,\overline{T}^{y}\delta_y h\right]_{i,j} = 0 \qquad (2.7)$$

For simplicity the convention of using the index pair (i,j) for the variable the equation of which is being considered is adopted here. In (2.6) and (2.7) y is carried at h-points and

$$\hat{h}^{(u)}_{i,j} \equiv (\overline{h}^{xyy})_{i,j}$$

$$\hat{F}^{(u)}_{i+\frac{1}{2},j} \equiv (\overline{F}^{xyy})_{i+\frac{1}{2},j} \qquad (2.8)$$

$$\hat{G}^{(u)}_{i,j+\frac{1}{2}} \equiv (\overline{G}^{xyy})_{i,j+\frac{1}{2}}$$

$$\hat{h}^{(v)}_{i,j} \equiv (\overline{h}^{xxy})_{i,j}$$

$$\hat{F}^{(v)}_{i+\frac{1}{2},j} \equiv (\overline{F}^{xxy})_{i+\frac{1}{2},j} \qquad (2.9)$$

$$\hat{G}^{(v)}_{i,j+\frac{1}{2}} \equiv (\overline{G}^{xxy})_{i,j+\frac{1}{2}}$$

$\hat{F}^{(u)}$, $\hat{G}^{(u)}$, $\hat{F}^{(v)}$ and $\hat{G}^{(v)}$ are new mass flux symbols, defined at the points shown in Figure 5 and 6.

Finally, the thermodynamic equation (1.23), retaining only the divergence terms, is at h-points represented as:

$$\frac{\partial}{\partial t}(hT)_{i,j} + \frac{1}{d^2}\left[F_{i+\frac{1}{2},j}\,\overline{T}^{x}_{i+\frac{1}{2},j} - F_{i-\frac{1}{2},j}\,\overline{T}^{x}_{i-\frac{1}{2},j}\right.$$

$$\left. + G_{i,j+\frac{1}{2}}\,\overline{T}^{y}_{i,j+\frac{1}{2}} - G_{i,j-\frac{1}{2}}\,\overline{T}^{y}_{i,j-\frac{1}{2}}\right] = 0 \qquad (2.10)$$

with F and G as in (2.5).

With equations (2.4), (2.6), (2.7) and (2.10), all integral constraints are satisfied. For a full derivation the reader is referred to the Annex.

## 2.3 Space differencing: the Laplace operator

For the discrete Laplace operator a five-point operator is used:

$$\nabla^2 A_{i,j} = \frac{A_{i+1,j} + A_{i-1,j} + A_{i,j+1} + A_{i,j-1} - 4A_{i,j}}{d^2} \qquad (2.11)$$

in which A represents any of the variables u, v and T.

## 2.4 The basin; boundary conditions

The basin is shown in Figure 7.
The eastern and western boundaries contain u-points while the northern and southern boundaries contain v-points only. At all boundaries no-slip and no-normal velocity conditions are applied as well as $\frac{\partial T}{\partial n} = 0$ (n defines outward normal direction).

## 2.5 Space differencing near the boundaries

The finite difference form of the momentum equations turns out to be too complicated for grid points at a distance less than d from the basin boundaries (the unshaded area in Figure 7) and has to be reconsidered. Summarizing the results, in the boundary area the relevant parts of (2.8) and (2.9) are to be simplified and replaced by:

$$\begin{aligned} \tilde{h}^{(u)}_{i,j} &= (\overline{h}^{x})_{i,j} \\ \tilde{F}^{(u)}_{i+\frac{1}{2}j} &= (\overline{F}^{x})_{i+\frac{1}{2}j} \end{aligned} \qquad (2.12)$$

$$\tilde{h}^{(v)}_{i,j} = (\overline{h}^{y})_{i,j}$$

$$\tilde{G}^{(v)}_{i,j+\frac{1}{2}} = (\overline{G}^{y})_{i,j+\frac{1}{2}} \qquad (2.13)$$

Furthermore the finite difference scheme for the Laplace-operator at u-, v- and T-points in this region now makes explicit use of the boundary conditions of section 2.4. How this is done, is shown here for a T-point near the southern boundary (see Figure 8):

$$\left(\frac{\partial T}{\partial y}\right)_{i,j+\frac{1}{2}} \equiv \frac{T_{i,j+1} - T_{i,j}}{d}$$

$$\left(\frac{\partial T}{\partial y}\right)_{i,j-\frac{1}{2}} = 0 \qquad \text{(boundary condition)}$$

$$\Rightarrow \left(\frac{\partial^2 T}{\partial y^2}\right)_{i,j} \rightarrow \frac{\left(\frac{\partial T}{\partial y}\right)_{i,j+\frac{1}{2}} - \left(\frac{\partial T}{\partial y}\right)_{i,j-\frac{1}{2}}}{d} = \frac{T_{i,j+1} - T_{i,j}}{d^2}$$

$$\left(\frac{\partial^2 T}{\partial x^2}\right)_{i,j} \rightarrow \frac{T_{i+1,j} + T_{i-1,j} - 2T_{i,j}}{d^2} \qquad \text{(if not near eastern or western boundary)}$$

$$\Rightarrow \nabla^2 T_{i,j} = \frac{T_{i+1,j} + T_{i-1,j} + T_{i,j+1} - 3T_{i,j}}{d^2} \qquad (2.14)$$

Compare this result with (2.11).

## 2.6 Damping at northern and southern boundaries

In the presence of boundaries the model equations allow the occurrence of coastally trapped waves. Arriving at the eastern boundary, an eastward travelling disturbance will transfer part of its energy to a northward and a southward travelling coastal wave, see Figure 9.
These waves will travel along the basin boundaries in the direction indicated in the Figure and arrive back at the equator at the western boundary. If both northern and southern boundary are purely artificial it is desirable to damp these disturbances. This is accomplished by adding a damping term of the form $-r(h-h^{\circ})$ to the equation of continuity at the h-points in the shaded area in Figure 9:

$$\frac{\partial h}{\partial t} + \frac{\partial hu}{\partial x} + \frac{\partial hv}{\partial y} = -r\,(h-h^{\circ}) + R_I \qquad (2.15)$$

in which r is a damping parameter and $h^\circ$ the undisturbed mixed layer thickness. r satifies (see Figure 9):

$$r = r_0 \frac{\|y\| - y_D}{(\frac{1}{2}L_y - y_D)} \qquad y_D \leq \|y\| \leq \tfrac{1}{2}L_y$$
$$r = 0 \qquad \|y\| < y_D \tag{2.16}$$

In the shaded area mechanical energy is added or removed by the damping term such that disturbances are effectively damped.
For consistency a similar term is added to the thermodynamic equation:

$$\frac{\partial hT}{\partial t} + \frac{\partial huT}{\partial x} + \frac{\partial hvT}{\partial y} = -rT\,(h-h^\circ) + R_{II} + \kappa h \nabla^2 T \tag{2.17}$$

The discretization of the new terms and $R_{I,II}$ at the RHS of (2.15) and (2.17) is straightforward.

## 2.7 Time differencing

The model equations can be written symbolically in the form:

$$\frac{\partial h}{\partial t} = f\,(h,\vec{A})$$
$$\frac{\partial h\vec{A}}{\partial t} = \vec{g}\,(h,\vec{A}) \tag{2.18}$$

The first of these represents the equation of continuity while the other one represents the flux form of the equation for each of the other variables.
For time differencing the leap-frog scheme is used:

$$\frac{h^{n+1} - h^{n-1}}{2\Delta t} = f\,(h^n,\vec{A}^n)$$
$$\frac{h^{n+1}\,\vec{A}^{n+1} - h^{n-1}\,\vec{A}^{n-1}}{2\Delta t} = \vec{g}\,(h^n,\vec{A}^n) \tag{2.19}$$

the superscripts denoting time levels.
The first step in a numerical integration is a forward one of time step $\Delta t$. In general form:

$$\frac{h^{n+1} - h^n}{\Delta t} = f\,(h^n, \vec{A}^n)$$

$$\frac{h^{n+1}\,\vec{A}^{n+1} - h^n\,\vec{A}^n}{\Delta t} = \vec{g}\,(h^n, \vec{A}^n) \qquad (2.20)$$

For reasons of convergence viscous terms and damping terms require forward time stepping. For these terms a forward time step of $2\Delta t$ is used. Periodically a time filter is applied to remove the computational mode.

# 3. SOME PRELIMINARY RESULTS

## 3.1 Introduction

In this final chapter results of some model experiments are presented. The first experiment has been designed to test mass and energy conservation properties of the finite difference scheme. In a second experiment the phase speed of reduced-gravity waves in the absence of planetary rotation($\beta$=0) has been tested. Finally, as an example of its present performance, the model response to a prescribed wind stress is shown.
In these experiments the effects of thermodynamics and of the parameterized exchange processes have all been neglected, i.e. $R_I = R_{II} = 0$ and T = constant.

## 3.2 Mass and energy conservation test

In order to test the mass and energy conservation properties of the finite difference scheme, an unforced, inviscid non-diffusive long-term integration has been performed. This was done for an initial mixed layer thickness perturbation h' satisfying $\int\int h' dxdy = 0$. The undisturbed mixed layer thicknesss h° is 200 m and initially u,v = 0.

Parameter settings were as follows:

| | | | |
|---|---|---|---|
| $L_x$ | = | 15,000 km | basin length |
| $L_y$ | = | 9,000 km | basin width |
| d | = | 150 km | grid size |
| $\Delta t$ | = | .125 day | time step |
| $\nu$ | = | 0 | eddy viscosity |
| $\kappa$ | = | 0 | eddy diffusivity |
| $r_0$ | = | 0 | damping parameter |
| $y_D$ | = | not specified | damping parameter |
| $\vec{\tau}$ | = | $\vec{0}$ | wind stress |
| T | = | 10 K | temperature difference |
| $\alpha$ | = | $3 * 10^{-4}$ $K^{-1}$ | thermal expansion coefficient |
| g | = | 9.8 m $sec^{-2}$ | acceleration of gravity |
| $\beta$ | = | $2.29 * 10^{-11}$ $m^{-1}$ $sec^{-1}$ | $\beta$ parameter |

With initial conditions as described above, equatorial waves are generated, carrying away the energy associated with the initial perturbation h'.
In Figure 10 it is shown how area-averaged potential and kinetic energy evolve with time. Total mechanical energy, i.e. the sum of potential and kinetic energy, is seen to be constant to a very good approximation.

The computations also showed that the relative mass increase of the model is less than $10^{-14}$ at day 100 (!).

### 3.3 Reduced gravity waves in the absence of planetary rotation

In the absence of planetary rotation the reduced-gravity wave speed is given by:

$$c = (g'h^\circ)^{\frac{1}{2}} \tag{3.1}$$

in which $g' = \alpha Tg$ (reduced-gravity) and $h^\circ$ is again the undisturbed mixed layer thickness.
With the parameter settings as in section 3.2, except for $h^\circ$ and d which here are 100 m and 375 km respectively, c is approximately 1.7 m $sec^{-1}$.

With an initial perturbation h' according to Figure 11a (and initially u,v = 0), gravity waves are expected to move radially out from the perturbation area. Mixed layer thickness perturbation contours at day 15 are shown in Figure 11b. The corresponding phase speed is found to be 150 km $day^{-1}$ which is approximately its theoretical value.

### 3.4 Response to a patch of westerly wind stress

In this section the model response to a patch of westerly wind stress is presented. The response is compared with the corresponding linear analytical solution obtained by Tang and Weisberg (1984). Two different wind stress forcings are considered. The first is a stationary patch of westerly wind stress near the western boundary. The second is different from the first in that it translates eastward along the equator with constant speed, starting near the western boundary.
In formula the wind stress is represented by:

$$\tau_x(x,y) = \tau_o e^{-(y/L_r)^2} [\theta(x-c_w t) - \theta(x-c_w t-x_0)] \qquad (3.2)$$

with

$\tau_0$ - amplitude

$L_r$ - equatorial Rossby radius
$L_r = (\alpha g T H_0)^{\frac{1}{4}} / \beta^{\frac{1}{2}}$

$c_w$ - eastward translation speed

$x_0$ - fetch parameter

$\theta(x)$ - step function: $\theta=0$ for $x<0$
$\theta=1$ for $x\geq 0$

Initial conditions are: $h = h^\circ = 213$ m, $u,v = 0$ in both experiments.
Parameter settings:

$L_x$ = 16,650 km (~ 150 degrees of longitude)
$L_y$ = 6,600 km
$d$ = 150 km
$\Delta t$ = .125 day
$\nu$ = 0
$\kappa$ = 0
$r_0$ = $2.5 * 10^{-6}$ $sec^{-1}$
$y_D$ = 2,850 km
$T$ = 10 K
$\alpha$ = $3 * 10^{-4}$ $K^{-1}$
$g$ = 9.8 m $sec^{-2}$
$\beta$ = $2.29 * 10^{-11}$ $m^{-1}$ $sec^{-1}$
$\tau_0$ = $10^{-6}$ N $m^{-2}$
$x_0$ = 4,500 km (~ 40 degrees of longitude)
$c_w$ = 0 $msec^{-1}$/.5 $msec^{-1}$

With the above choice of parameters the Kelvin wave speed is 2.5 m $sec^{-1}$ and the equatorial Rossby radius $L_r$ is about 330 km. Choosing $\tau_0$ as small as $10^{-6}$ N $m^{-2}$, the response can be considered linear to a very good approximation.

Experiment 1: Response to a stationary patch of westerly wind stress ($c_w$ = 0 $msec^{-1}$)

In Figure 12 mixed layer thickness perturbation contours for a 400 days' integration are shown at intervals of 25 days. The forced region at the west side is easily recognized throughout the integration period and so is the phenomenon of equatorial trapping. An eastward travelling Kelvin wave is excited which impinges on the eastern boundary after about 60 days, its energy being carried away by a number of Rossby waves with westward group velocity and a pair of poleward travelling coastally trapped waves which upon arrival in the region at the northern and southern boundary are damped.

Figure 13 shows mixed layer thickness perturbation and zonal velocity on the equator as a function of longitude and time. The forcing region, Kelvin and Rossby waves are all easily discernable in the contours. From the slope of the Kelvin wave contours (lower right of either (a) or (b)) the Kelvin wave speed is found to be approximately 2.5 $msec^{-1}$, which equals its theoretical value. The reflected Rossby waves are particularly clear in Figure 13b. At day 325 a reflected Kelvin wave is seen to emerge from the forcing region in Figure 13a.

In Figure 14 finally mixed layer thickness perturbation and zonal velocity are shown as a function of time at an equatorial point 30 degrees of longitude to the west of the eastern boundary. In the same Figure the approximate linear analytical solution at this point (from Tang and Weisberg (1984)) is shown. In finding an analytical solution Tang and Weisberg used the long-wave approximation. This approximation eliminates coastally trapped waves and the waves that are retained are non-dispersive (e.g. Knox and Anderson (1985)). Bearing this in mind we now compare the solutions shown in Figure 14a, in which arrows mark changes in slope of the analytical solution (dashed line).

The first arrow marks the day of arrival of the leading edge of a Kelvin wave response. Downwelling thereafter is exactly reproduced by the model. At day 62 ($2^{nd}$ arrow) the trailing edge of this Kelvin wave arrives, together with the leading edge of an upwelling Kelvin wave originating at the western boundary as a reflection of the Rossby wave response. From this point the model upwelling speed is slightly smaller than its analytical value. After day 100 changes in slope of the analytical solution are attributed to the arrival and passage of reflected Rossby waves generated at the eastern boundary, the third and fifth arrow marking the day of arrival of the n = 1 and 3 Rossby mode respectively.

Differences between model and analytical response after day 100 are in qualitative agreement with the fact that the Rossby waves generated in the model are dispersive. The effects of coastally trapped waves, absent when the long wave approximation is employed, are less clear.

Experiment 2: Response to an eastward translating patch of westerly wind stress ($c_w$ = .5 msec$^{-1}$)

In Figure 15 mixed layer thickness perturbation and zonal velocity on the equator are shown as a function of longitude and time. Figure 16 shows the corresponding analytical solutions from Tang and Weisberg (1984). The forced region, translating eastward here, Kelvin and Rossby waves are again easily recognized. Apart from some minor differences, close agreement between model and analytical response is observed.
Figure 17 finally corresponds to Figure 13, but now for the eastward translating wind stress. For a discussion the reader is referred to experiment 1, Figure 13.

## 4. CONCLUSIONS

A baroclinic two-layer ocean model on an equatorial β-plane has been described. It is an extension of the usual reduced-gravity model in that it includes active thermodynamics.

The model equations are discretized on an Arakawa-C grid. Special attention has been paid to mass and energy conservation requirements on the finite difference scheme.

Preliminary experiments have shown satisfactory results. The model will be used in experiments with coupled equatorial ocean-atmosphere models.

## ACKNOWLEDGMENTS

The author would like to thank Theo Opsteegh and Robert Mureau for their close guidance.

Special thanks to Marleen Kaltofen and Birgit Kok for typing the manuscript and Matty Brouwer for preparing the figures.

ANNEX: SPACE DIFFERENCING AND INTEGRAL CONSTRAINTS

In this Annex the details of the finite difference scheme are discussed. A space difference scheme is set up that has mass and energy conservation properties outlined in section 1.3. The basis for the present scheme has been taken from Haltiner et al. (1979). Notes on this scheme by Arakawa et al. (1977) are partly reproduced. All equations are discretized in their unforced, inviscid, non-diffusive form:

$$\frac{\partial hu}{\partial t} + \frac{\partial huu}{\partial x} + \frac{\partial huv}{\partial y} - \beta yhv = - \tfrac{1}{2}\alpha g \frac{\partial}{\partial x}(h^2 T) \qquad (A.1)$$

$$\frac{\partial hv}{\partial t} + \frac{\partial hvu}{\partial x} + \frac{\partial hvv}{\partial y} + \beta yhu = - \tfrac{1}{2}\alpha g \frac{\partial}{\partial y}(h^2 T) \qquad (A.2)$$

$$\frac{\partial h}{\partial t} + \frac{\partial hu}{\partial x} + \frac{\partial hv}{\partial y} = 0 \qquad (A.3)$$

$$\frac{\partial hT}{\partial t} + \frac{\partial huT}{\partial x} + \frac{\partial hvT}{\partial y} = 0 \qquad (A.4)$$

The equation of continuity in finite difference form is chosen on the basis of simplicity. At h-points (A.3) is represented as

$$\frac{\partial}{\partial t} h_{i,j} + \frac{1}{d^2}[\delta_x F + \delta_y G]_{i,j} = 0 \qquad (A.5)$$

with the mass fluxes

$$F_{i+\frac{1}{2},j} = d\,[\overline{h}^{x} u]_{i+\frac{1}{2},j}$$
$$G_{i,j+\frac{1}{2}} = d\,[\overline{h}^{y} v]_{i,j+\frac{1}{2}} \qquad (A.6)$$

defined at u- and v-points respectively (see Figure 4).
Averaging and difference operators are defined at the beginning of section 2.2.
With (A.5) mass conservation is guaranteed in a relatively simple way. Another requirement on the finite difference scheme is that it conserve total kinetic energy during inertial processes.
Now first consider the first three terms at the LHS of (A.1). These can be represented by the following form which automatically ensures that integrated zonal momentum (in the absence of boundaries) is conserved.

$$\frac{\partial}{\partial t}(\tilde{h}^{(u)} u)_{i,j} + \frac{1}{d^2}[\delta_x (\tilde{F}^{(u)}\,\overline{u}^{x}) + \delta_y (\tilde{G}^{(u)}\,\overline{u}^{y})]_{i,j} \qquad (A.7)$$

in which $\tilde{h}^{(u)}$, $\tilde{F}^{(u)}$ and $\tilde{G}^{(u)}$ are as yet undefined. The latter two are new mass flux symbols defined at the points shown in Figure 5.

Again the convention of using the index pair (i,j) for the variable the equation of which is being considered is adopted. Choosing $\tilde{h}^{(u)}$, $\tilde{F}^{(u)}$ and $\tilde{G}^{(u)}$ in such a way that they satisfy

$$\frac{\partial}{\partial t} \tilde{h}^{(u)}_{i,j} + \frac{1}{d^2} [\delta_x \tilde{F}^{(u)} + \delta_y \tilde{G}^{(u)}]_{i,j} = 0 \qquad (A.8)$$

it can be shown that (A.7), by subtracting (A.8) multiplied by $u_{i,j}$ is equivalent to:

$$\tilde{h}^{(u)}_{i,j} \frac{\partial u_{i,j}}{\partial t} + \frac{1}{d^2} [\overline{\tilde{F}^{(u)}}^{x} \delta_x u + \overline{\tilde{G}^{(u)}}^{y} \delta_y u]_{i,j} \qquad (A.9)$$

Multiplying (A.9) by $u_{i,j}$ and combining with (A.8), multiplied by $\frac{1}{2}u^2_{i,j}$, yields a discrete analogon to the first two terms of the total kinetic energy equation (1.28):

$$\frac{\partial}{\partial t} (\tilde{h}^{(u)} \tfrac{1}{2}u^2)_{i,j} + \frac{1}{2d^2} [\tilde{F}^{(u)}_{i+\frac{1}{2},j} u_{i,j} u_{i+1,j} - \tilde{F}^{(u)}_{i-\frac{1}{2},j} u_{i-1,j} u_{i,j}$$

$$+ \tilde{G}^{(u)}_{i,j+\frac{1}{2}} u_{i,j} u_{i,j+1} - \tilde{G}^{(u)}_{i,j-\frac{1}{2}} u_{i,j+1} u_{i,j}] \qquad (A.10)$$

Summing (A.10) over i, flux terms at one grid point turn out to be cancelled by contributions from neighbouring grid points. Thus, regardless of the precise definition of $\tilde{h}^{(u)}$, $\tilde{F}^{(u)}$ and $\tilde{G}^{(u)}$, the choice of form (A.7) and the constraint (A.8) together ensure that total kinetic energy does not spuriously increase of decrease.

Next we define $\tilde{h}^{(u)}$, $\tilde{F}^{(u)}$ and $\tilde{G}^{(u)}$ as follows:

$$\begin{aligned} \tilde{h}^{(u)}_{i,j} &\equiv (\overline{h}^{xyy})_{i,j} \\ \tilde{F}^{(u)}_{i+\frac{1}{2},j} &\equiv (\overline{F}^{xyy})_{i+\frac{1}{2},j} \\ \tilde{G}^{(u)}_{i,j+\frac{1}{2}} &\equiv (\overline{G}^{xyy})_{i,j+\frac{1}{2}} \end{aligned} \qquad (A.11)$$

definitions satisfying (A.8), using (A.5).

Similar arguments apply to the first three terms of (A.2).
Their finite difference form is simply found by replacing u by v in (A.7):

$$\frac{\partial}{\partial t}\,(\tilde{h}^{(v)}\ v)_{i,j} + \frac{1}{d^2}\,[\delta_x\,(\tilde{F}^{(v)}\ \overline{v}^{x}) + \delta_y\,(\tilde{G}^{(v)}\ \overline{v}^{y})]_{i,j} \tag{A.12}$$

in which (cf. (A.11) and see Figure 6 for points of definition):

$$\begin{aligned}
\tilde{h}^{(v)}_{i,j} &\equiv (\overline{h}^{xxy})_{i,j} \\
\tilde{F}^{(v)}_{i+\frac{1}{2},j} &\equiv (\overline{F}^{xxy})_{i+\frac{1}{2},j} \\
\tilde{G}^{(v)}_{i,j+\frac{1}{2}} &\equiv (\overline{G}^{xxy})_{i,j+\frac{1}{2}}
\end{aligned} \tag{A.13}$$

The Coriolis term $-\beta yhv$ in (A.1) is at the u point (i,j) represented by:

$$-\beta(\overline{yh\overline{v}^{y}}^{x})_{i,j} \tag{A.14}$$

and the term $\beta yhu$ in (A.2) at the v-point $(i+\frac{1}{2},j+\frac{1}{2})$ by

$$\beta\,(\overline{yh\overline{u}^{x}}^{y})_{i+\frac{1}{2},j+\frac{1}{2}} \tag{A.15}$$

Here y is carried at h-points.

The rate of change of zonal kinetic energy at the u-point (i,j) by the Coriolis force is found by multiplying (A.14) by $u_{i,j}$. The contribution to this from the v-point $(i+\frac{1}{2},j+\frac{1}{2})$ is found to be:

$$-\tfrac{1}{4}\beta y_j\ h_{i+\frac{1}{2},j}\ v_{i+\frac{1}{2},j+\frac{1}{2}}\ u_{i,j} \tag{A.16}$$

Analogously the change of meridional kinetic energy at the v-point $(i+\frac{1}{2},j+\frac{1}{2})$ is found by multiplying (A.15) by $v_{i+\frac{1}{2},j+\frac{1}{2}}$. The fraction due to the u-point (i,j) equals:

$$\tfrac{1}{2}\ \beta y_j\ h_{i+\frac{1}{2},j}\ u_{i,j}\ v_{i+\frac{1}{2},j+\frac{1}{2}} \tag{A.17}$$

(A.16) and (A.17) exactly cancel so that total kinetic energy is not influenced by the Coriolis terms.

Before examining the pressure gradient terms, we discretize the thermodynamic equation (A.4) as follows

$$\begin{aligned}
&\frac{\partial(hT)}{\partial t}_{i,j} + \frac{1}{d^2}\,[F_{i+\frac{1}{2},j}\ \overline{T}^{x}_{i+\frac{1}{2},j} - F_{i-\frac{1}{2},j}\ \overline{T}^{x}_{i-\frac{1}{2},j} \\
&+ G_{i,j+\frac{1}{2}}\ \overline{T}^{y}_{i,j+\frac{1}{2}} - G_{i,j-\frac{1}{2}}\ \overline{T}^{y}_{i,j-\frac{1}{2}}] = 0
\end{aligned} \tag{A.18}$$

with F and G defined by (A.6). This form can be shown to guarantee the conservation of enthalpy in a closed region as follows.

Summing (A.18) over all grid points, cancelling of flux terms at every grid point by neighbouring grid point contributions occurs, showing $\Sigma(hT)_{i,j}$ is a conserved quantity. Recalling $T = T_1 - T_2$ and $T_2$ is constant, mass conservation, $\frac{\partial}{\partial t} \Sigma h_{i,j} = 0$, can be used to show that $\Sigma(hT_1)_{i,j}$, i.e. the total enthalpy of the upper layer (see (1.27) for definition), too is a conserved quantity, as required.

The finite difference form of the pressure gradient must satisfy the requirement that no spurious energy production takes place or, equivalently, that the conversion of potential to kinetic energy and vice versa will be such that no energy constraint is violated.

At h-points (T-points) we define the potential energy as $\frac{1}{2}h_{i,j}{}^2T_{i,j}$ (cf. (1.26)). An equation for the rate of change with time of this quantity is easily found by combining (A.5) and (A.18). Ignoring for the moment the meridional terms:

$$\begin{aligned}\frac{\partial(\frac{1}{2}h^2T)}{\partial t}_{i,j} + \frac{1}{d}\Big[ & \tfrac{1}{4}h_{i,j}\,T_{i,j}\,(h_{i,j} + h_{i+1,j})\,u_{i+\frac{1}{2},j} \\ & - \tfrac{1}{4}h_{i,j}\,T_{i,j}\,(h_{i,j} + h_{i-1,j})\,u_{i-\frac{1}{2},j}\Big] \\ + \frac{1}{d}\Big[ & \tfrac{1}{8}h_{i,j}\,(h_{i,j} + h_{i+1,j})\,(T_{i,j} + T_{i+1,j})\,u_{i+\frac{1}{2},j} \\ & - \tfrac{1}{8}h_{i,j}\,(h_{i,j} + h_{i-1,j})\,(T_{i,j} + T_{i-1,j})\,u_{i-\frac{1}{2},j}\Big] = 0\end{aligned} \tag{A.19}$$

In this equation contributions from the u-points $(i+\frac{1}{2},j)$ and $(i-\frac{1}{2},j)$ can be recognized. Now we restrict our attention to the contribution from $u_{i+\frac{1}{2},j}$. It can be shown that further contributions of $u_{i+\frac{1}{2},j}$ to potential energy changes are confined to the h point (i+1,j):

$$\begin{aligned}\frac{\partial(\frac{1}{2}h^2T)_{i+1,j}}{\partial t} + \frac{1}{d}\Big[ & \tfrac{1}{4}h_{i+1,j}\,T_{i+1,j}\,(h_{i+1,j} + h_{i+2,j})\,u_{i+\frac{3}{2},j} \\ & - \tfrac{1}{4}h_{i+1,j}\,T_{i+1,j}\,(h_{i+1,j} + h_{i,j})\,u_{i+\frac{1}{2},j}\Big] \\ + \frac{1}{d}\Big[ & \tfrac{1}{8}h_{i+1,j}\,(h_{i+1,j} + h_{i+2,j})\,(T_{i+1,j} + T_{i+2,j})\,u_{i+\frac{3}{2},j} \\ & - \tfrac{1}{8}h_{i+1,j}\,(h_{i+1,j} + h_{i,j})\,(T_{i+1,j} + T_{i,j})\,u_{i+\frac{1}{2},j}\Big] = 0\end{aligned} \tag{A.20}$$

The total contribution of $u_{i+\frac{1}{2},j}$ to the potential energy changes at $h_{i+1,j}$ and $h_{i,j}$ is given by the sum of the underlined terms in (A.19) and (A.20).

$$\frac{1}{d}\Big[\tfrac{1}{4}h_{i,j}\,T_{i,j}\,(h_{i,j}+h_{i+1,j}) - \tfrac{1}{4}h_{i+1,j}\,T_{i+1,j}\,(h_{i+1,j}+h_{i,j}) + \tfrac{1}{8}h_{i,j}\,(h_{i,j}+h_{i+1,j})\,(T_{i,j}+T_{i+1,j}) - \tfrac{1}{8}h_{i+1,j}\,(h_{i+1,j}+h_{i,j})\,(T_{i+1,j}+T_{i,j})\Big] * u_{i+\frac{1}{2},j}$$

or:

$$\frac{u_{i+\frac{1}{2},j}}{2d}\left[\overline{h}^{x}_{i+\frac{1}{2},j}\,\delta_x\,(hT)_{i+\frac{1}{2},j} + \overline{h}^{x}_{i+\frac{1}{2},j}\,\overline{T}^{x}_{i+\frac{1}{2},j}\,\delta_x\,(h)_{i+\frac{1}{2},j}\right] \qquad (A.21)$$

In the absence of external sources the production of zonal kinetic energy at $u_{i+\frac{1}{2},j}$ equals the rate of doing work by the zonal component of the pressure gradient at $u_{i+\frac{1}{2},j}$. Apart from a constant factor:

$$-u_{i+\frac{1}{2},j}\left[\frac{\partial}{\partial x}\tfrac{1}{2}h^2T\right]_{i+\frac{1}{2},j} \qquad (A.22)$$

We now require the sum of (A.21) and (A.22) to be identically zero, providing the finite difference form of the pressure gradient (its zonal component):

$$\frac{\partial}{\partial x}(\tfrac{1}{2}h^2T) \rightarrow \left[\tfrac{1}{2}\overline{h}^{x}_{i+\frac{1}{2},j}\,\delta_x(hT)_{i+\frac{1}{2},j} + \tfrac{1}{2}\overline{h}^{x}_{i+\frac{1}{2},j}\,\overline{T}^{x}_{i+\frac{1}{2},j}\,\delta_x(h)_{i+\frac{1}{2},j}\right]/d \qquad (A.23)$$

Its differential analogon is equivalent to the statement that $\frac{\partial}{\partial x}(\frac{1}{2}h^2T)$ can be written as:

$$\frac{\partial}{\partial x}(\tfrac{1}{2}h^2T) = \tfrac{1}{2}h\,\frac{\partial hT}{\partial x} + \tfrac{1}{2}hT\,\frac{\partial h}{\partial x}$$

Similar arguments yield the finite difference form of $\frac{\partial}{\partial y}(\frac{1}{2}h^2T)$ at $v_{i,j+\frac{1}{2}}$ (the meridional component of the pressure gradient):

$$\frac{\partial}{\partial y}(\tfrac{1}{2}h^2T) \rightarrow \left[\tfrac{1}{2}\overline{h}^{y}_{i,j+\frac{1}{2}}\,\delta_y(hT)_{i,j+\frac{1}{2}} + \tfrac{1}{2}\overline{h}^{y}_{i,j+\frac{1}{2}}\,\overline{T}^{y}_{i,j+\frac{1}{2}}\,\delta_y(h)_{i,j+\frac{1}{2}}\right]/d \qquad (A.24)$$

REFERENCES

Anderson, D.L.T. and McCreary, J.P. (1985). Slowly propagating disturbances in a coupled ocean-atmosphere model, J. Atm. Sc., 42, 615-629.

Arakawa, A. and Lamb, V.R. (1977). Computational design of the basic dynamical processes of the UCLA General Circulation Model, Methods in Comp. Physics, 17, 173-265.

Gill, A.E. (1982). Atmosphere-Ocean Dynamics, Academic Press New York, 662 pp.

Haltiner, G.J. and Williams, R.T. (1979). Numerical Prediction and Dynamic Meteorology (2nd ed.), John Wiley and Sons New York et al., 477 pp.

Knox, R.A. and Anderson, D.L.T. (1985). Recent advances in the study of the low-latitude ocean circulation, Prog. Oceanog., 14, 259-317.

Tang, T.Y. and Weisberg, R.H. (1984). On the equatorial Pacific response to the 1982/1983 El Niño-Southern Oscillation event, J. of Mar. Res., 42, 809-829.

FIGURE CAPTIONS

Figure 1: Two-layer ocean model, vertical cross section.

Figure 2: Compensation of the effects of a sloping free surface for the baroclinic mode. (a) $h_1$ constant; $\frac{\partial \eta_1}{\partial x} < 0$, $\frac{\partial T}{\partial x} < 0$

(b) T constant; $\frac{\partial \eta_1}{\partial x} < 0$, $\frac{\partial h_1}{\partial x} < 0$.

Figure 3: The Arakawa-C grid. T is defined at h-points and the grid size is d.

Figure 4: Grid showing points of definition of mass fluxes in the equation of continuity.

Figure 5: Grid showing points of definition of mass fluxes in the zonal momentum equation.

Figure 6: Grid showing points of definition of mass fluxes in the meridional momentum equation.

Figure 7: The basin. The outer boundary is the basin boundary. Modification of the space difference scheme is necessary for grid points between basin boundary and shaded interior.

Figure 8: Grid points involved in the discretization of the Laplace-operator at a T-point in the southern boundary area.

Figure 9: Coastally trapped waves. Damping takes place in the shaded areas ($y_D < \|y\| < \frac{1}{2}L_y$).

Figure 10: Evolution of potential (middle solid line), zonal kinetic (dashed line), meridional (lower solid line) and total mechanical (upper solid line) energy for the mass-and-energy conservation test.

Figure 11: Reduced-gravity waves for a non-rotating earth. The initial mixed layer thickness perturbation is shown in (a) (units are m). In (b) contours of thickness perturbation are shown after 15 days (units are m).

Figure 12: Evolution of mixed layer thickness perturbation for a stationary westerly wind stress of amplitude $10^{-6}$ N $m^{-2}$ defined by equation (3.2) and a 400 days' integration period shown at intervals of 25 days (units are $10^{-5}$ m).

Figure 13: (a) Equatorial mixed layer thickness perturbation as a function of time for a stationary westerly wind stress of amplitude $10^{-6}$ N $m^{-2}$ defined by equation (3.2) (units are $10^{-5}$ m).
(b) Equatorial zonal velocity component perturbation as a function of time for the same wind stress as in (a) (units are $10^{-5}$ cm $sec^{-1}$).

Figure 14: (a) Equatorial mixed layer thickness perturbation at 110 W as a function of time for a westerly wind stress of amplitude $10^{-6}$ N $m^{-2}$ defined by equation (3.2).
Dashed line represents approximate linear analytical solution (from Tang and Weisberg (1984)), solid line represents model response.
(b) Same as (a) but for zonal velocity component.

Figure 15 (a) As Figure 13a, but for a wind stress that translates eastward at a rate $c_w$ = .5 msec$^{-1}$.
(b) As Figure 13b, but for a wind stress as in (a).

Figure 16 (a) As Figure 15a, but from Tang and Weisberg (1984) (analytical solution).
(b) As Figure 15b, but from Tang and Weisberg (1984) (analytical solution).

Figure 17 (a) As Figure 14a but for a wind stress that translates eastward at a rate $c_w$ = .5 msec$^{-1}$.
(b) As Figure 14b, but for a wind stress as in (a).

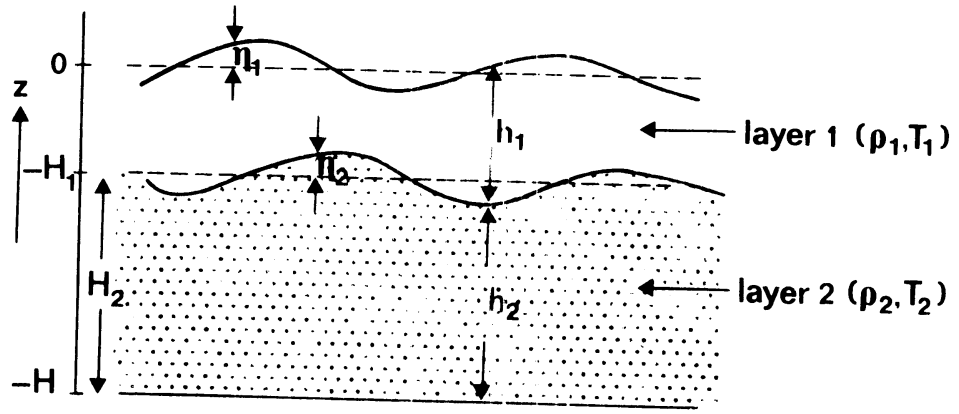


figure 1

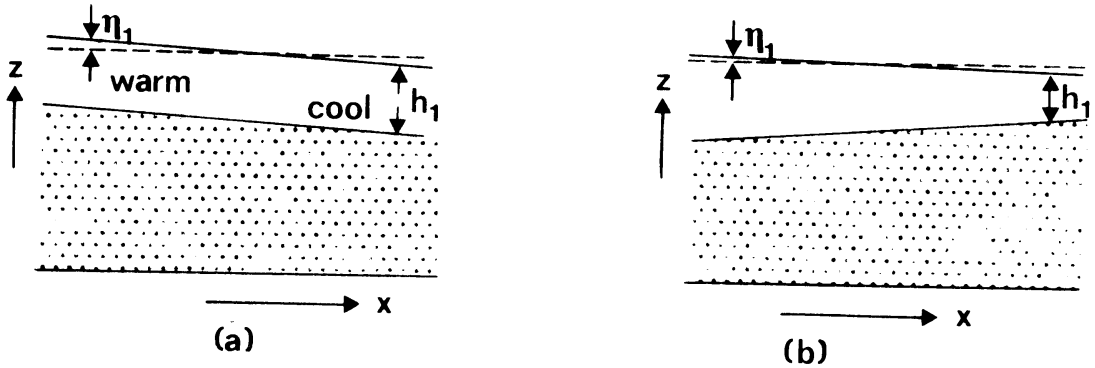


figure 2

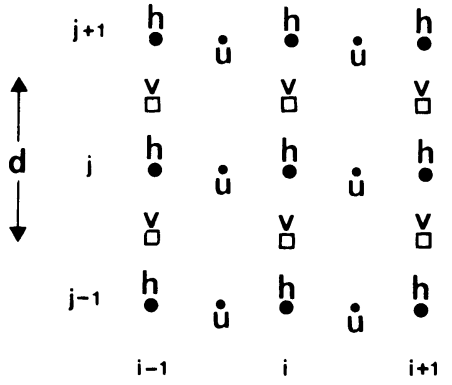


figure 3

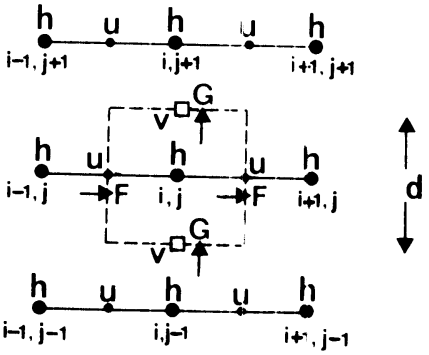


figure 4

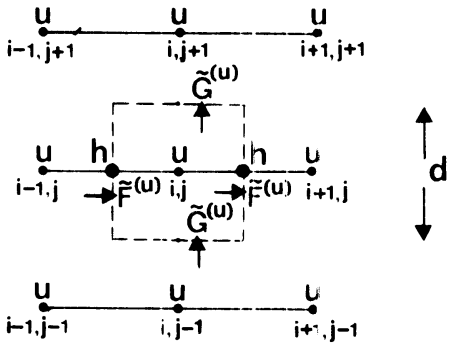


figure 5

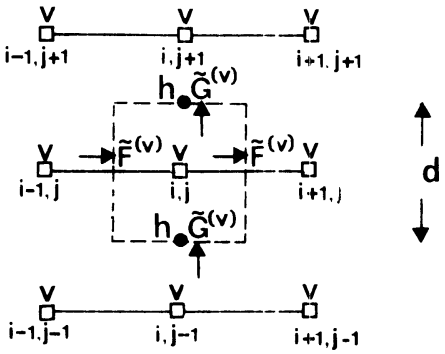


figure 6

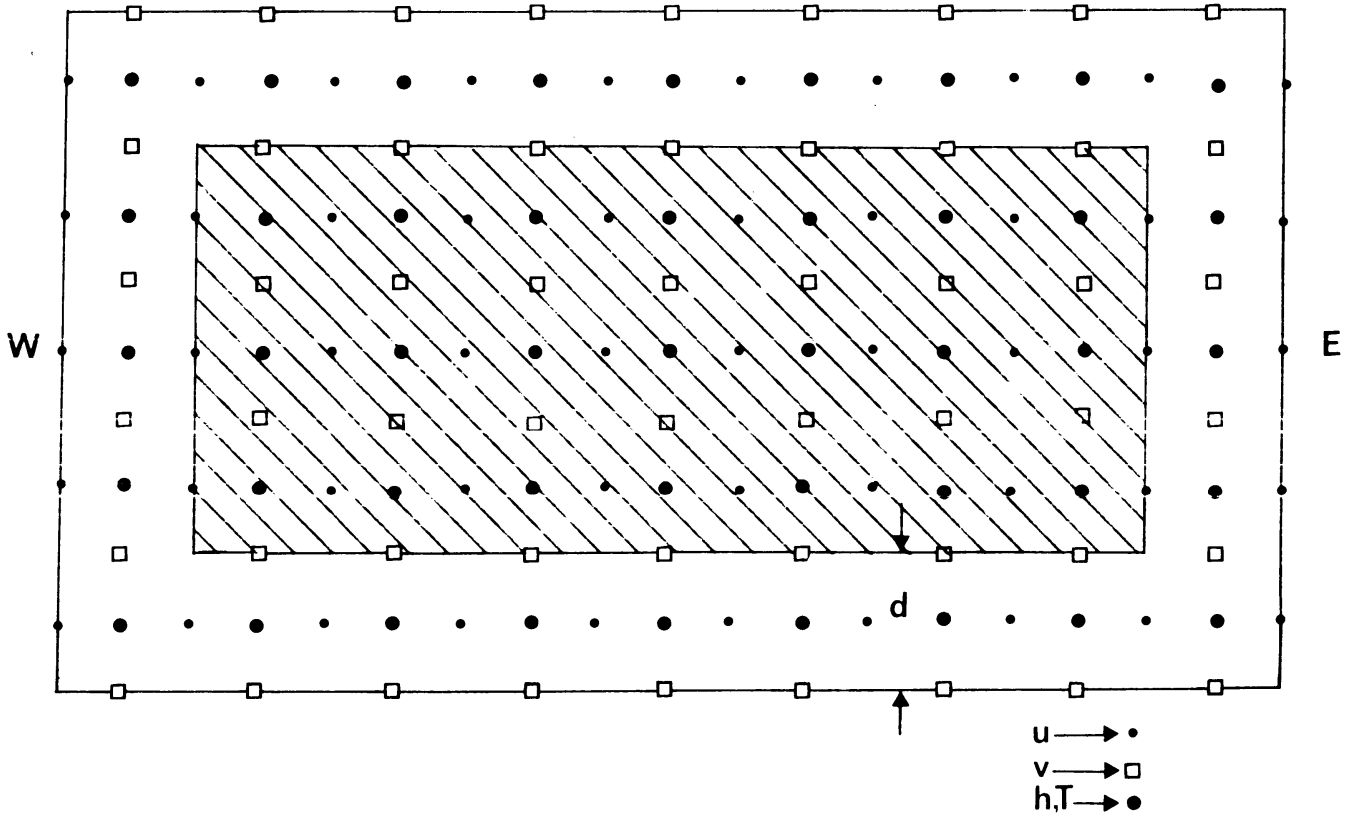


figure 7

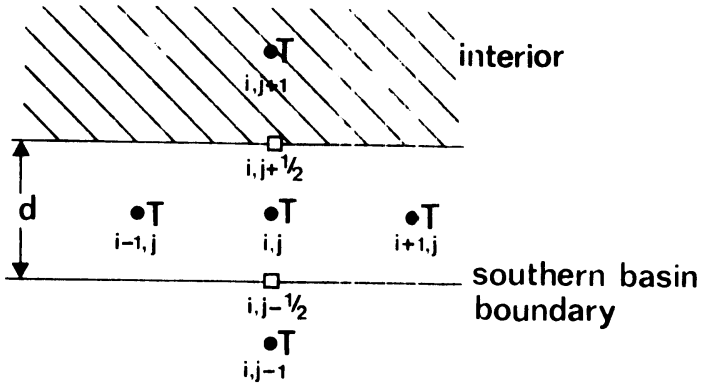


figure 8

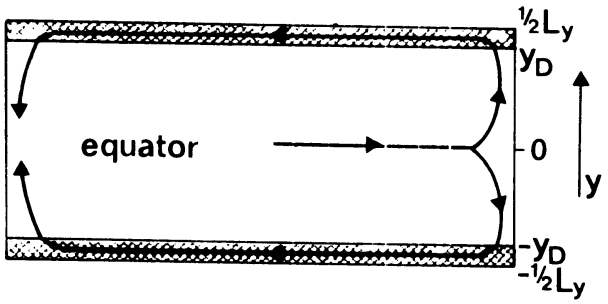


figure 9

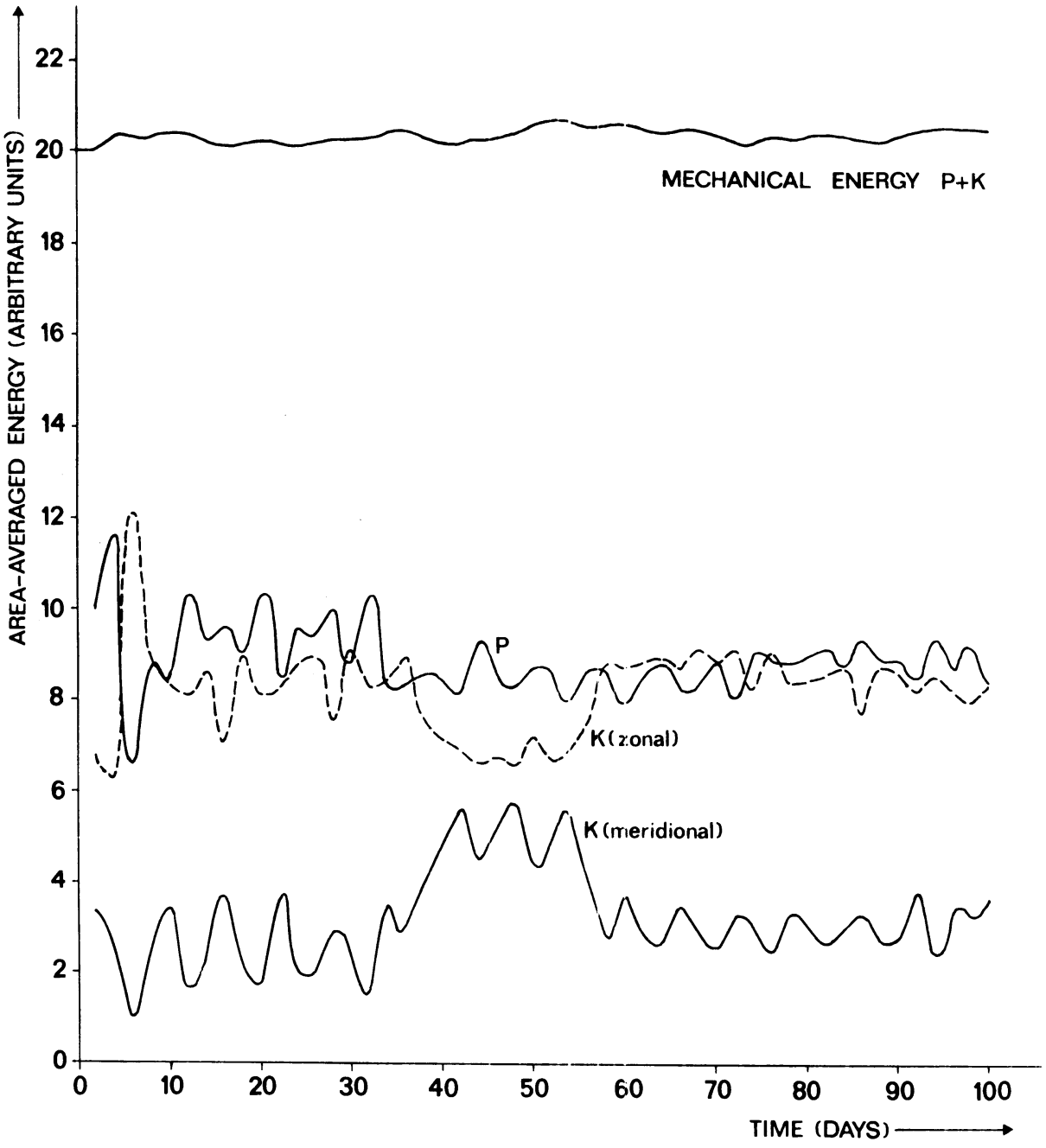
AREA-AVERAGED ENERGY (ARBITRARY UNITS)
22
20
18
16
14
12
10
8
6
4
2
0
MECHANICAL ENERGY P+K
P
K (zonal)
K (meridional)
0
10
20
30
40
50
60
70
80
90
100
TIME (DAYS)

figure 10

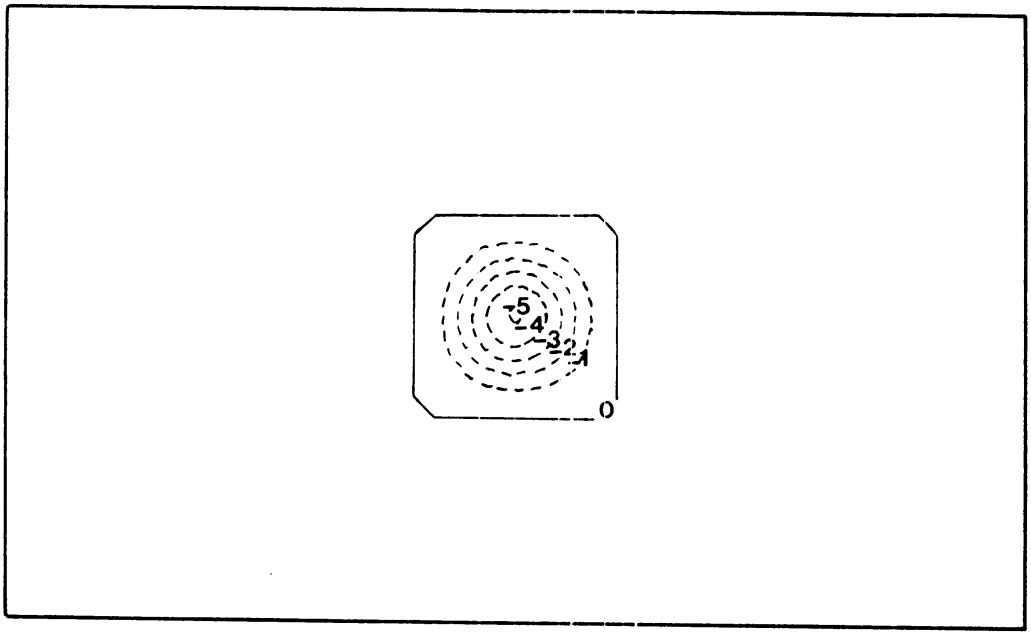


figure 11a

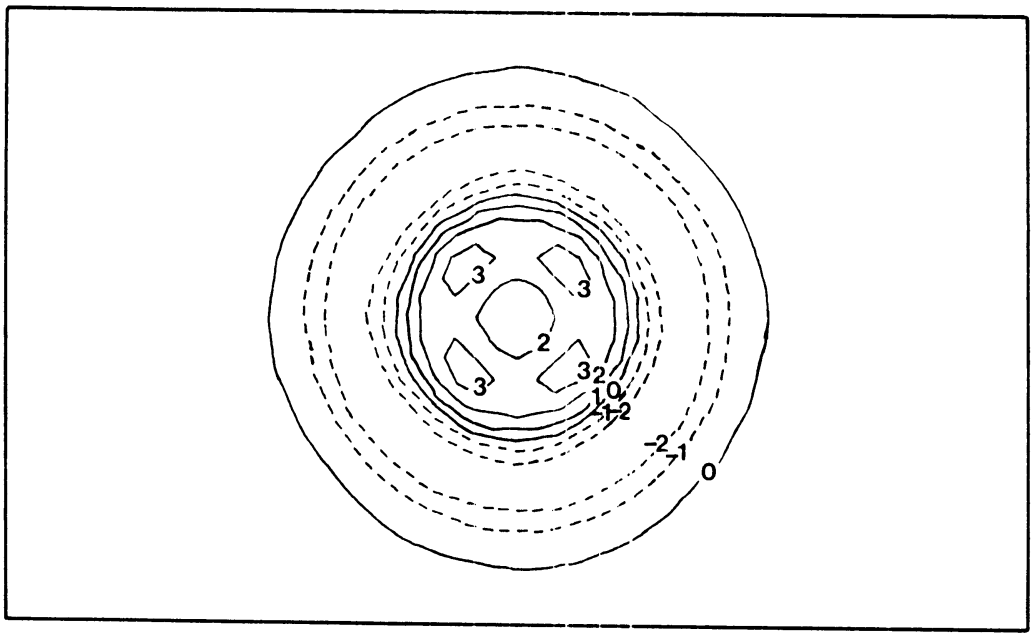


figure 11b

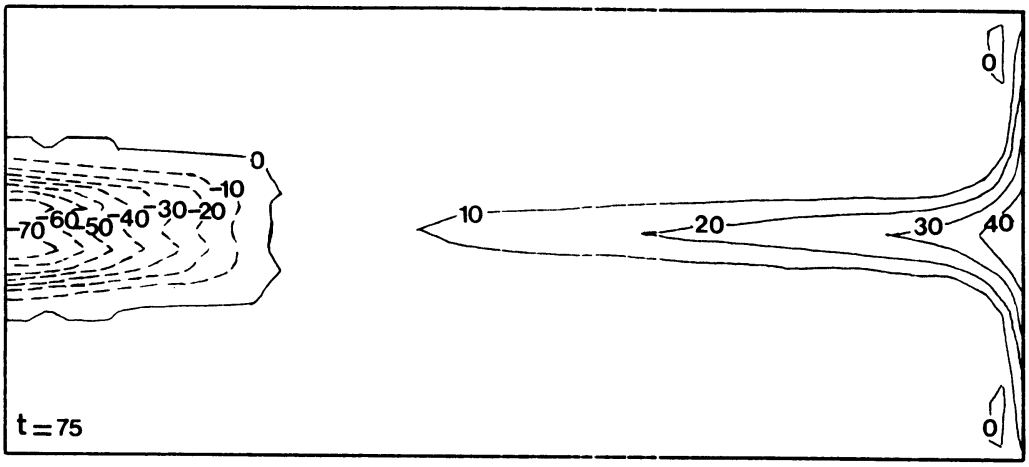
0
-10
-70 -60 -50 -40 -30 -20
10
20
30
40
0
t=75

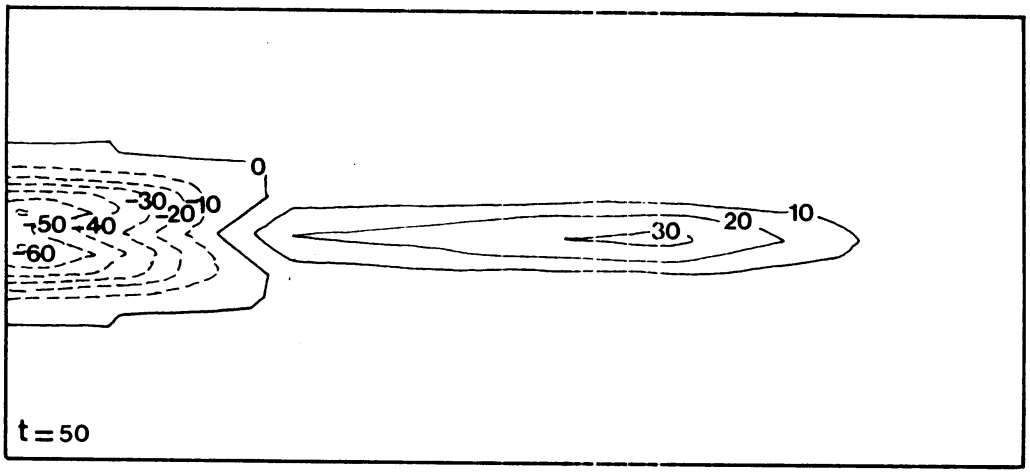
0
-30 -20 10
-50 -40
-60
30
20
10
t=50

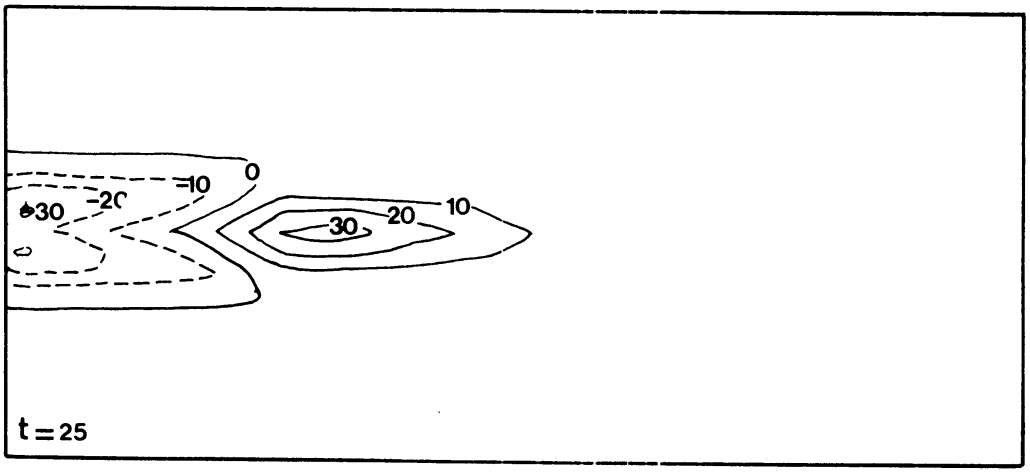
0
-10
-30 -20
30
20
10
t=25

figure 12

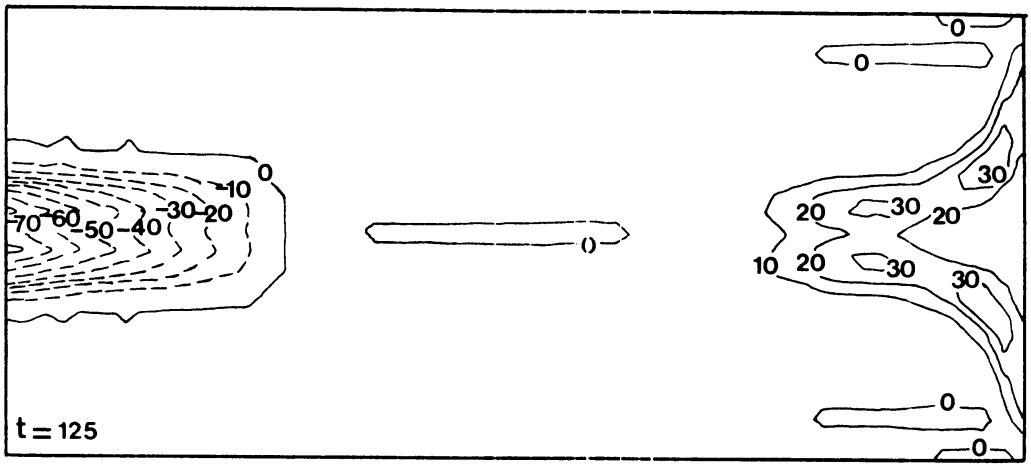


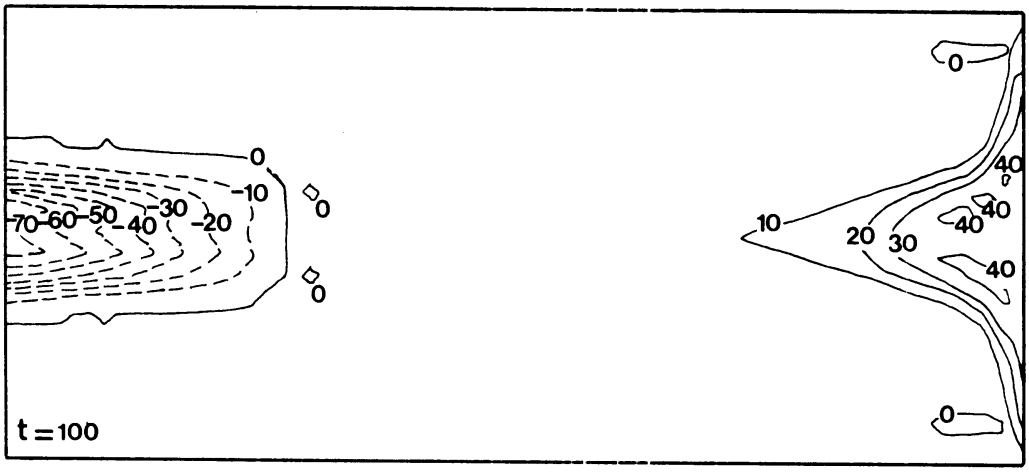


figure 12 (continued)

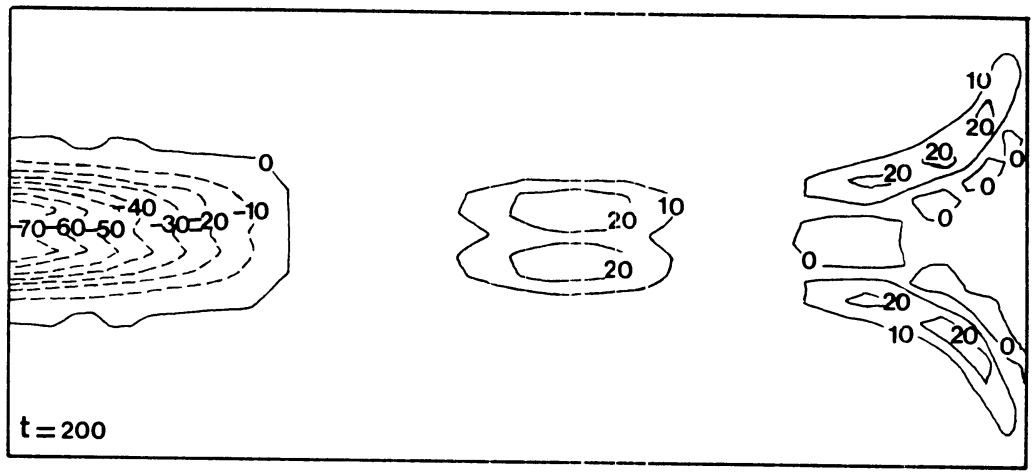


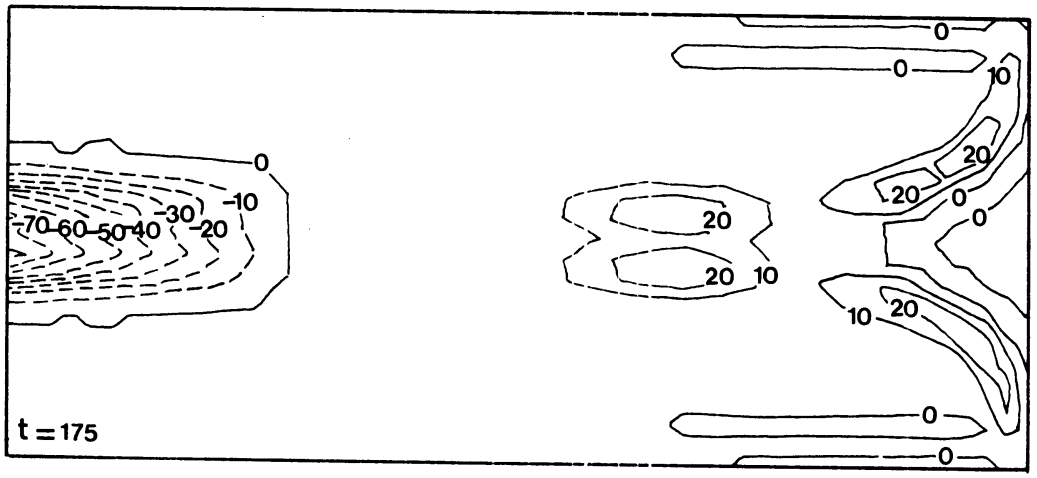


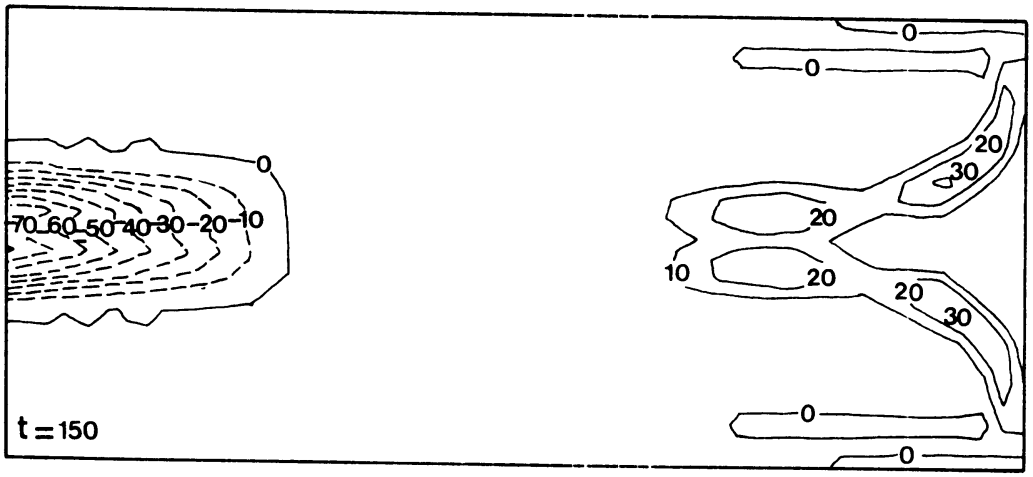


figure 12 (continued)

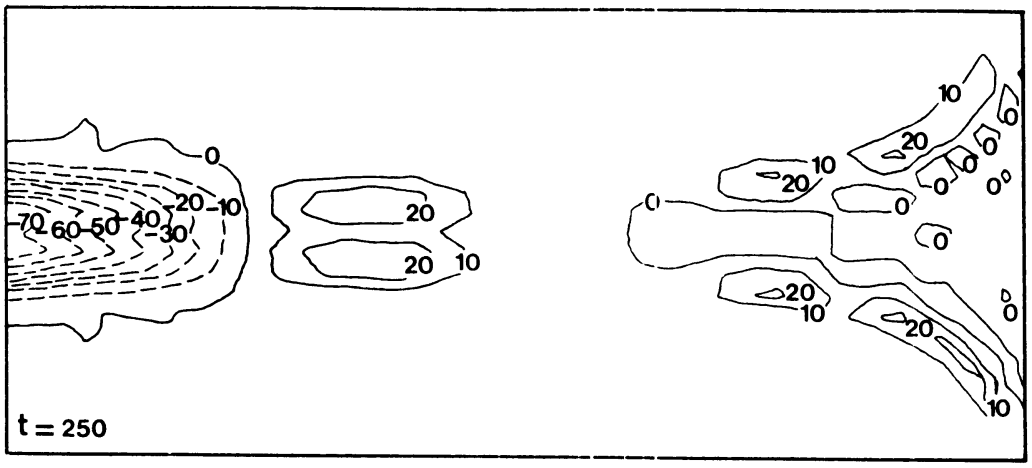


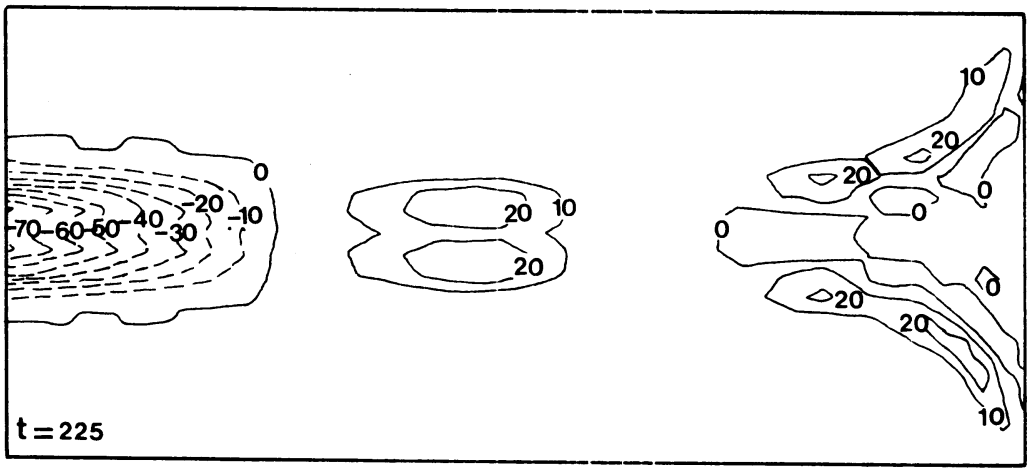


figure 12 (continued)

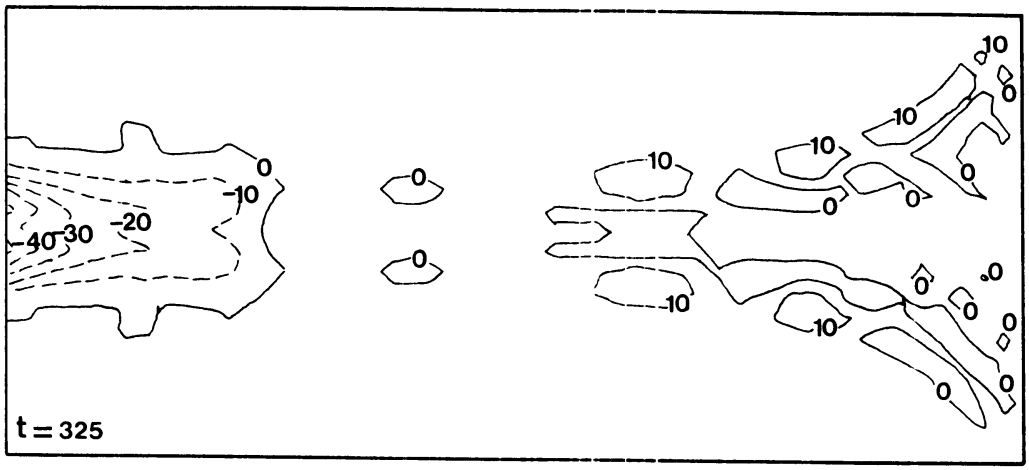


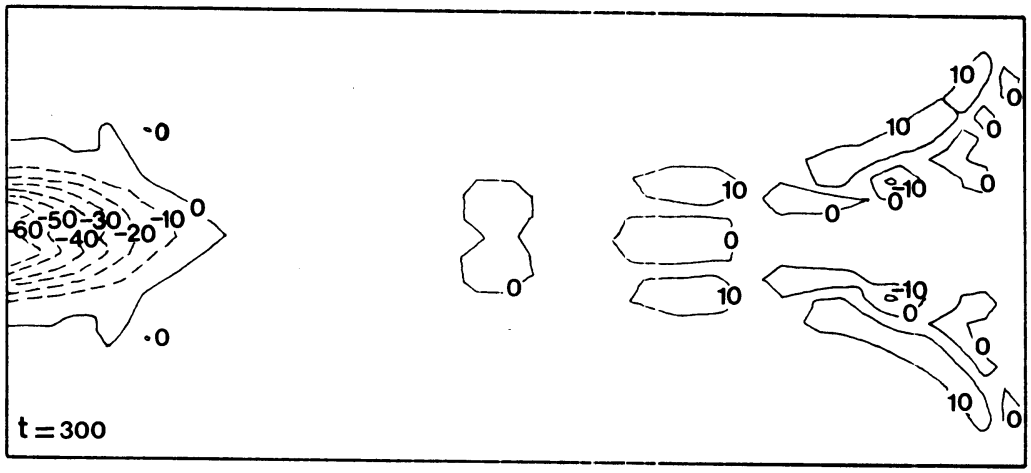


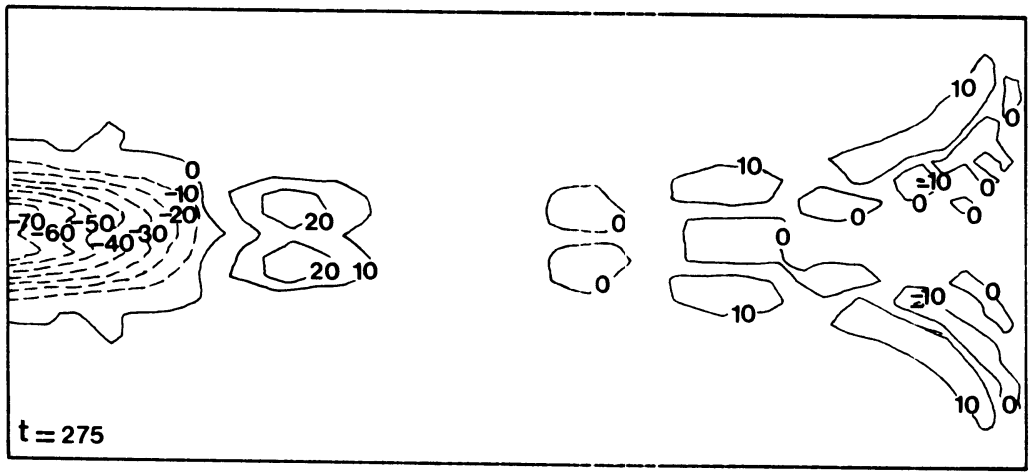


figure 12 (continued)

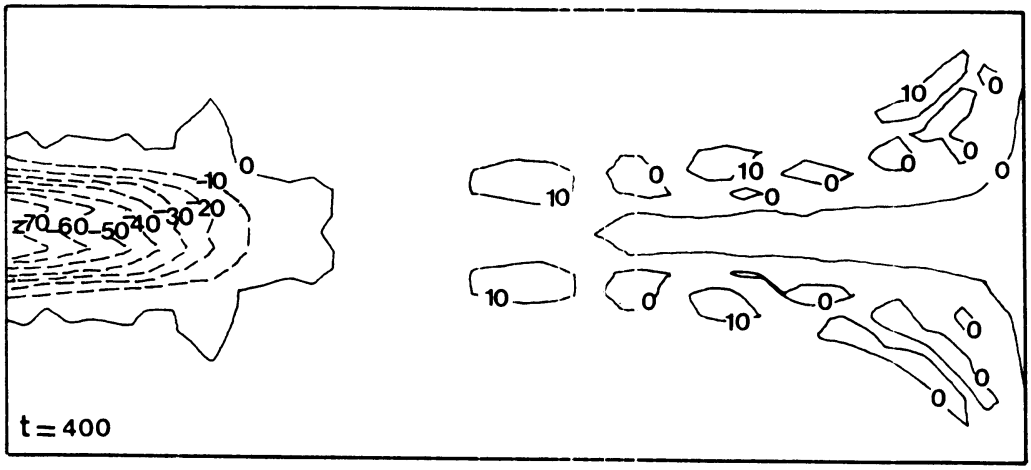


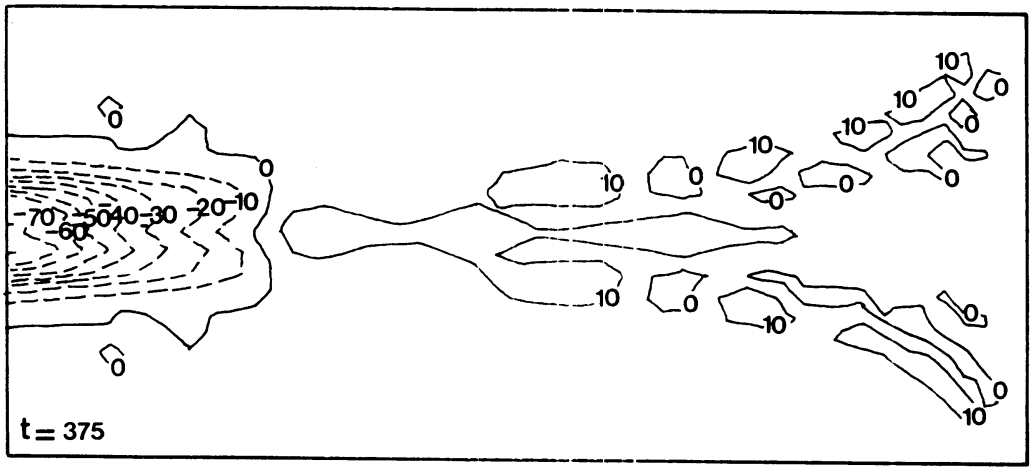


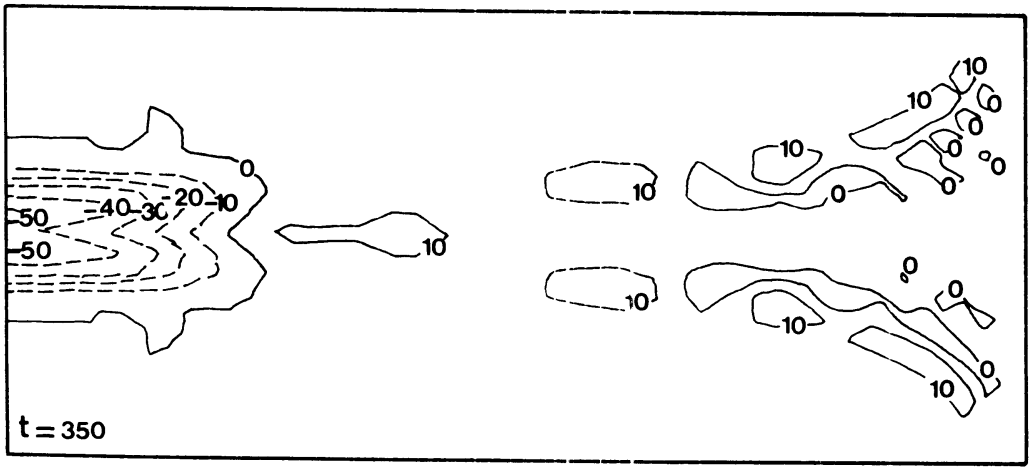


figure 12 (continued)

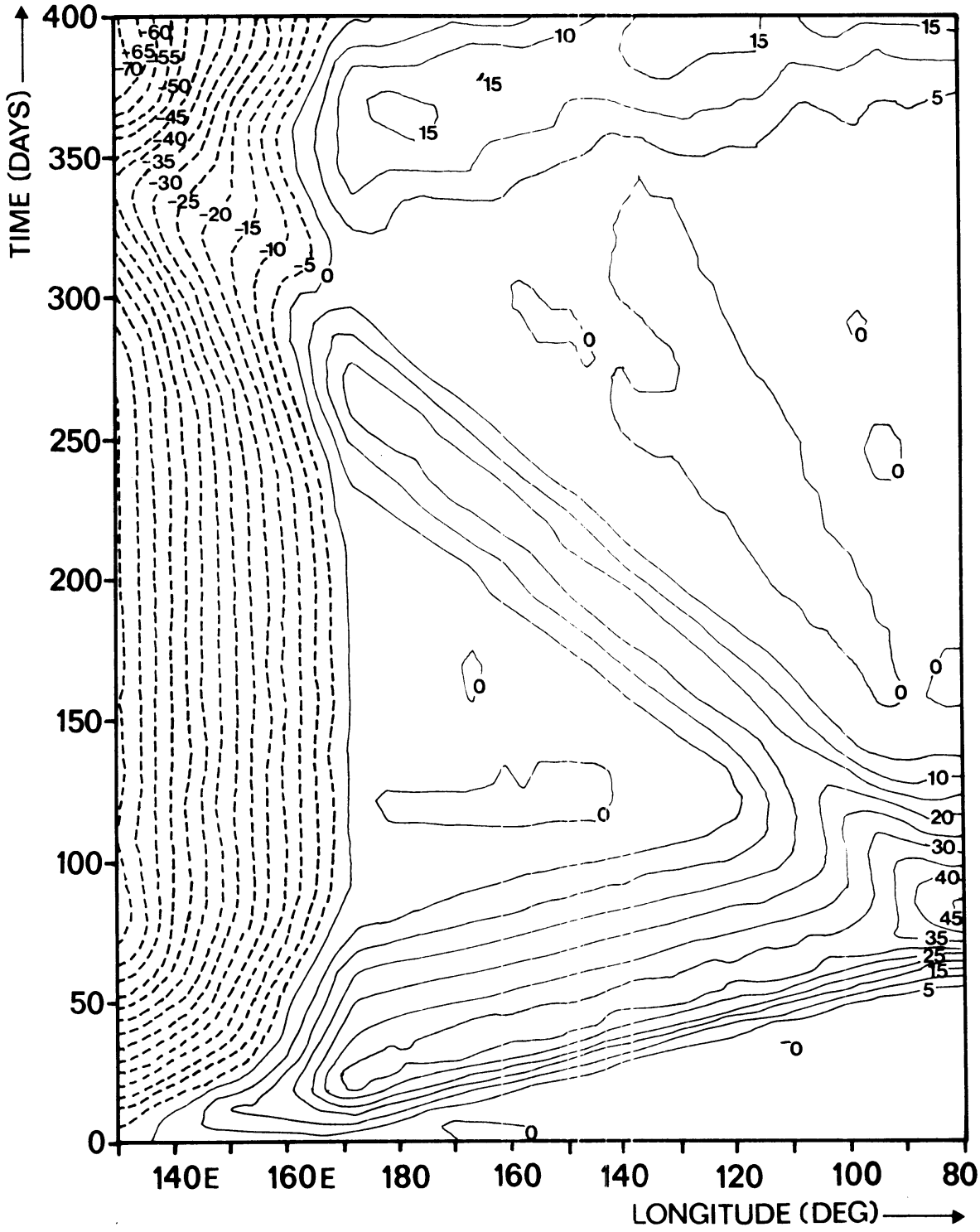
TIME (DAYS)
400
350
300
250
200
150
100
50
0
140E
160E
180
160
140
120
100
80
LONGITUDE (DEG)

figure 13 (a)

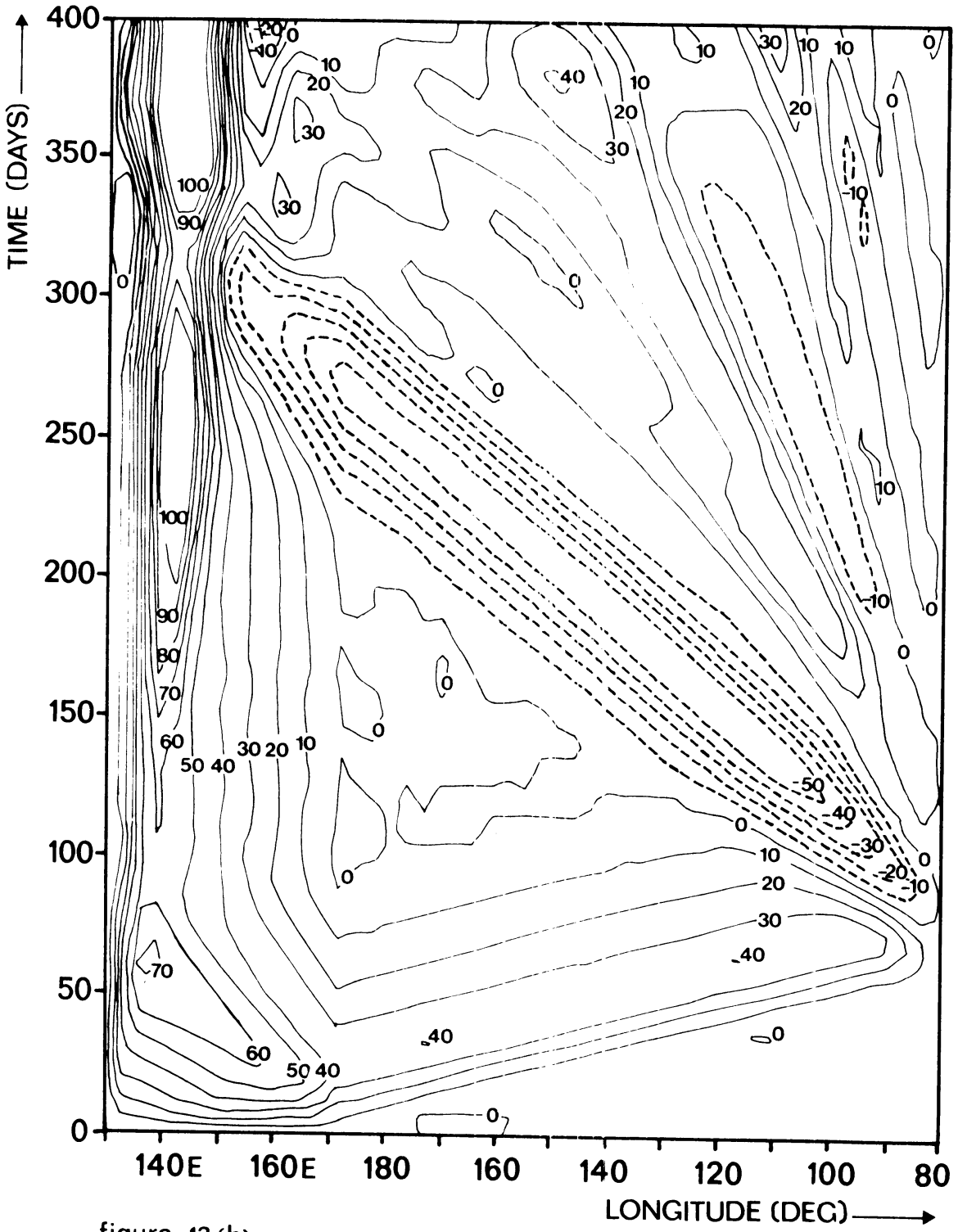
TIME (DAYS)
400
350
300
250
200
150
100
50
0
140E
160E
180
160
140
120
100
80
LONGITUDE (DEG)

figure 13 (b)

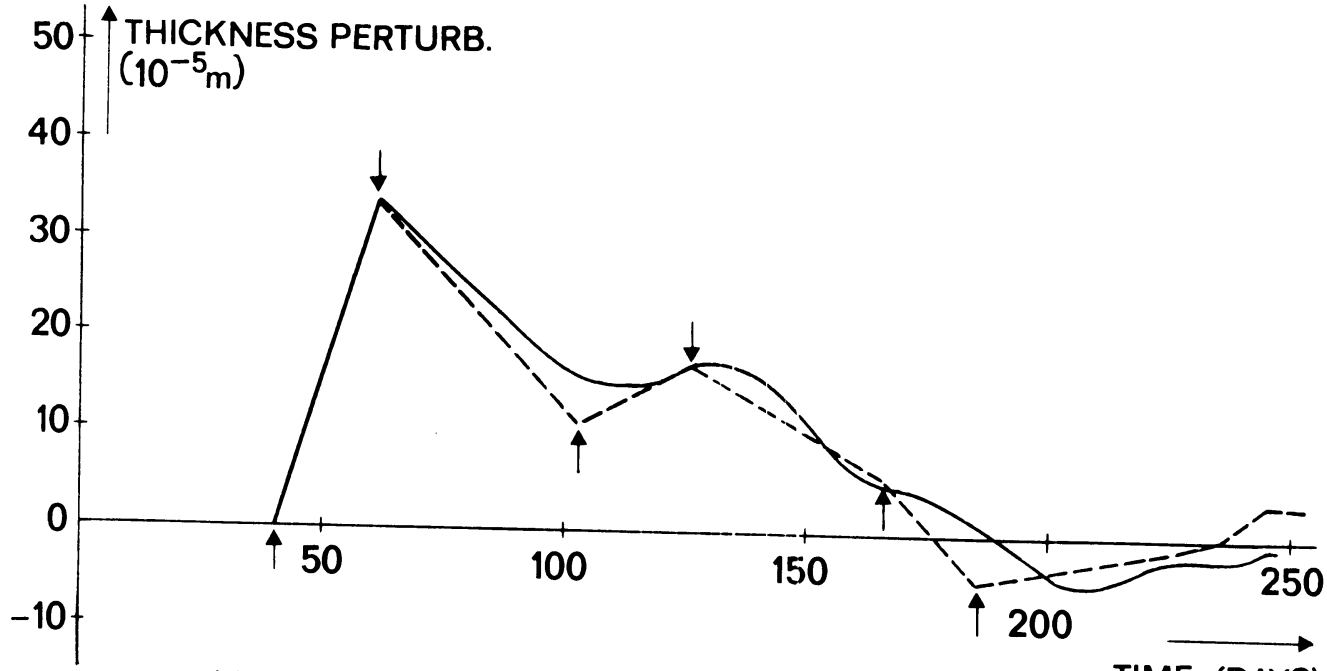


figure 14(a)

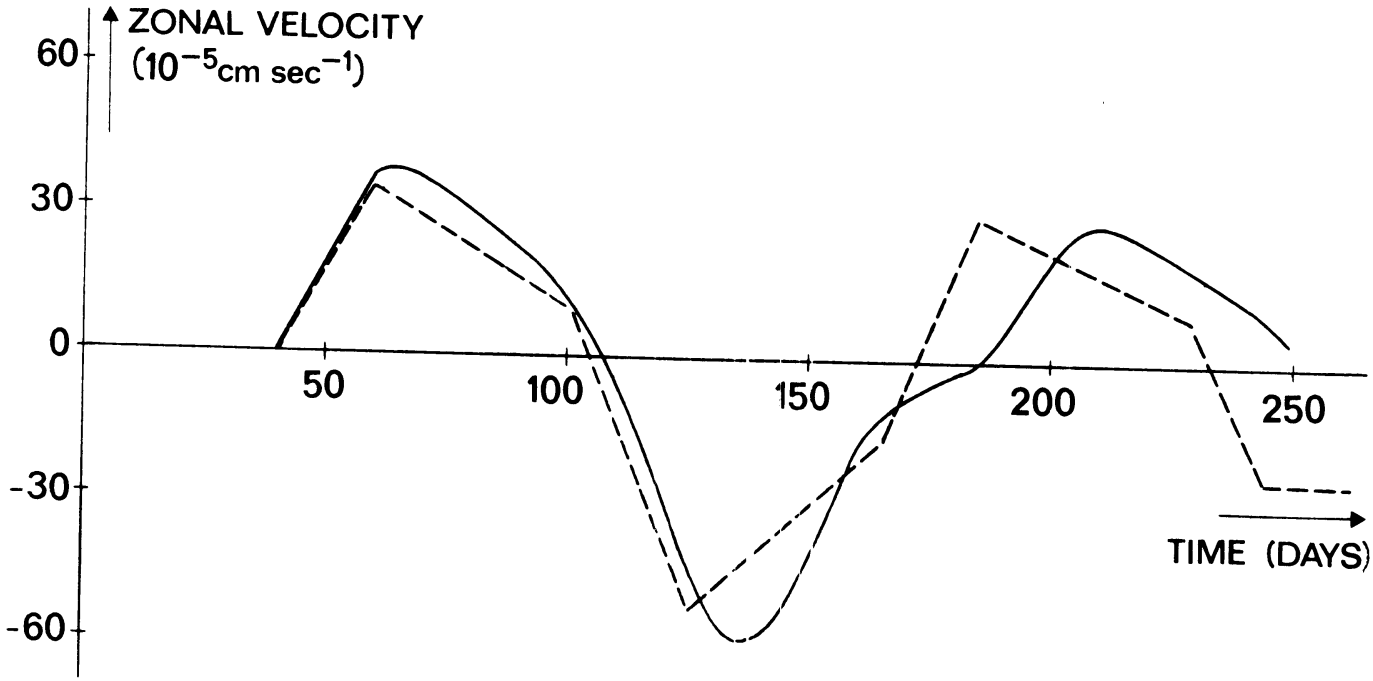


figure 14 (b)

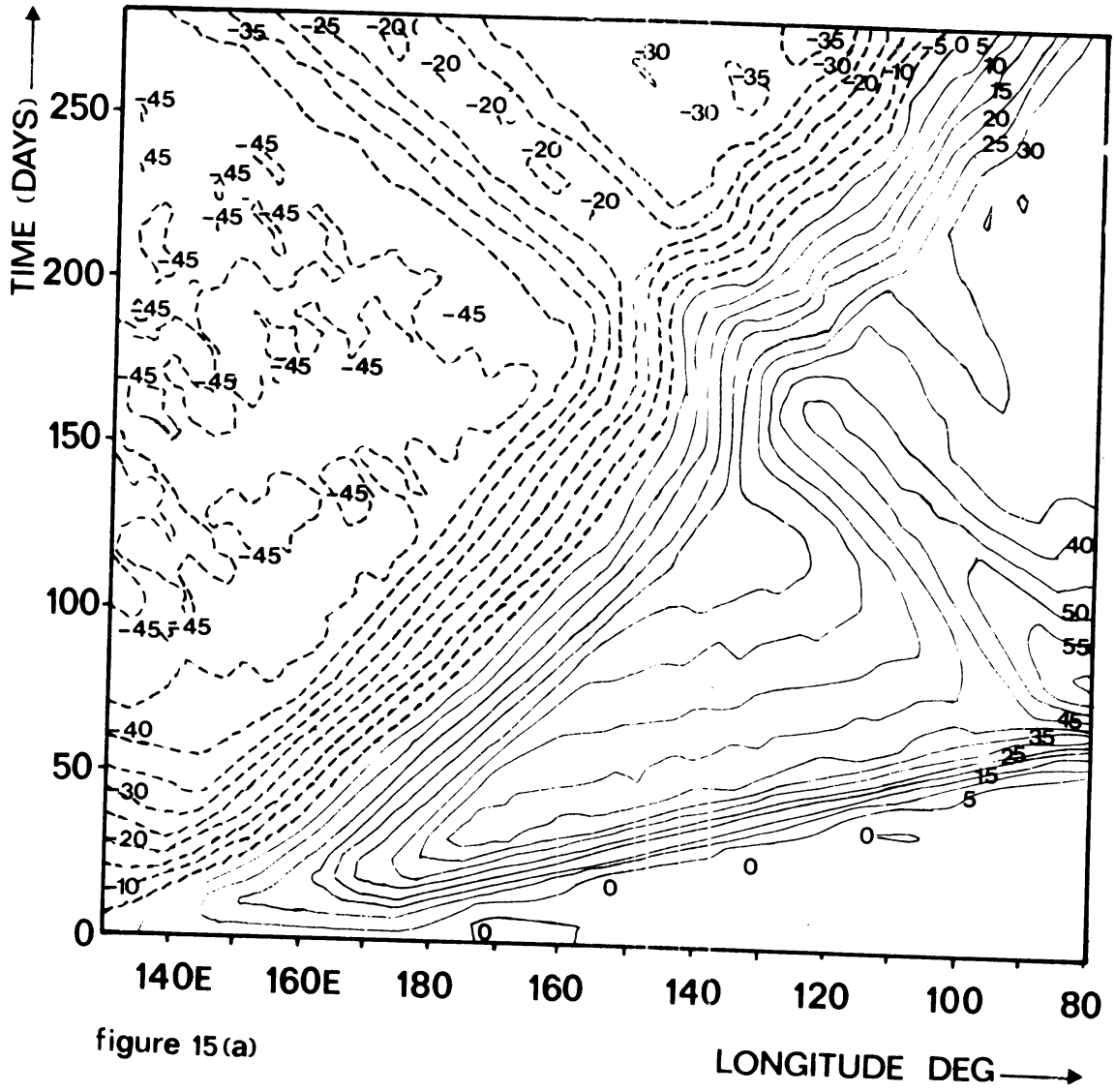
TIME (DAYS)
250
200
150
100
50
0
140E
160E
180
160
140
120
100
80
LONGITUDE DEG

figure 15(a)

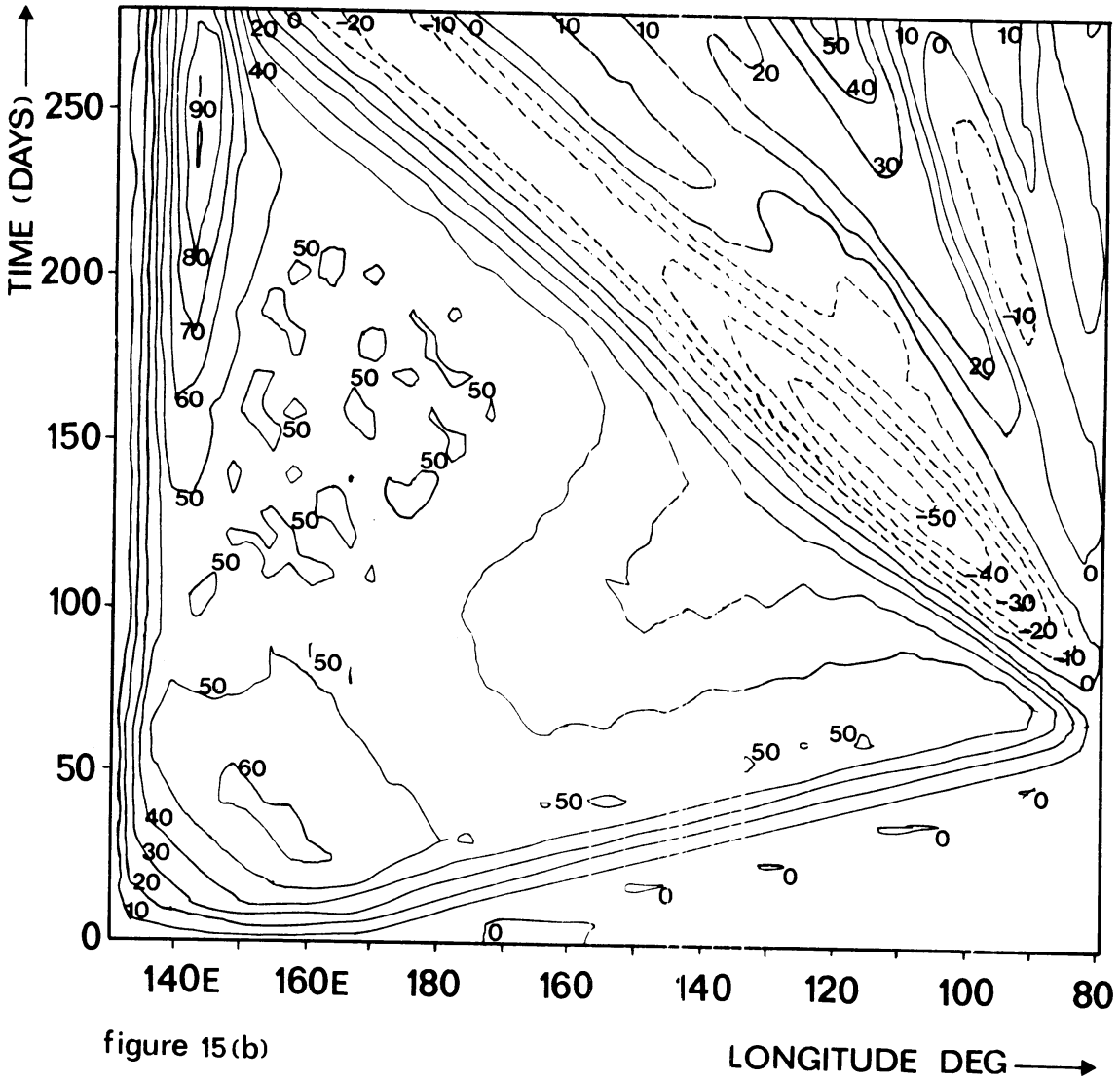
TIME (DAYS)
250
200
150
100
50
0
140E
160E
180
160
140
120
100
80
LONGITUDE DEG

figure 15(b)

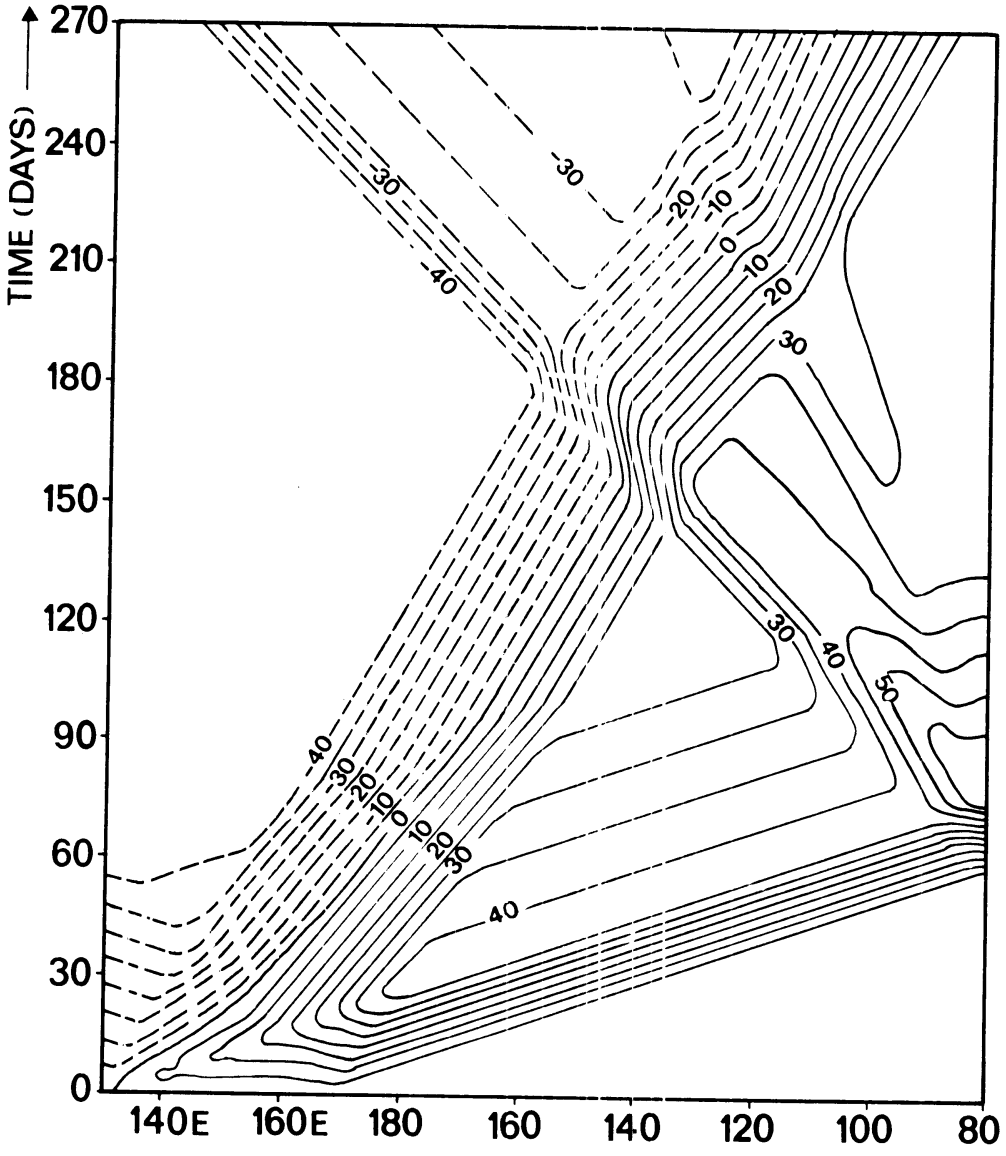
TIME (DAYS)
270
240
210
180
150
120
90
60
30
0
140E
160E
180
160
140
120
100
80
LONGITUDE (DEG)
-40
-30
-20
-10
0
10
20
30
40
50

figure 16 (a)

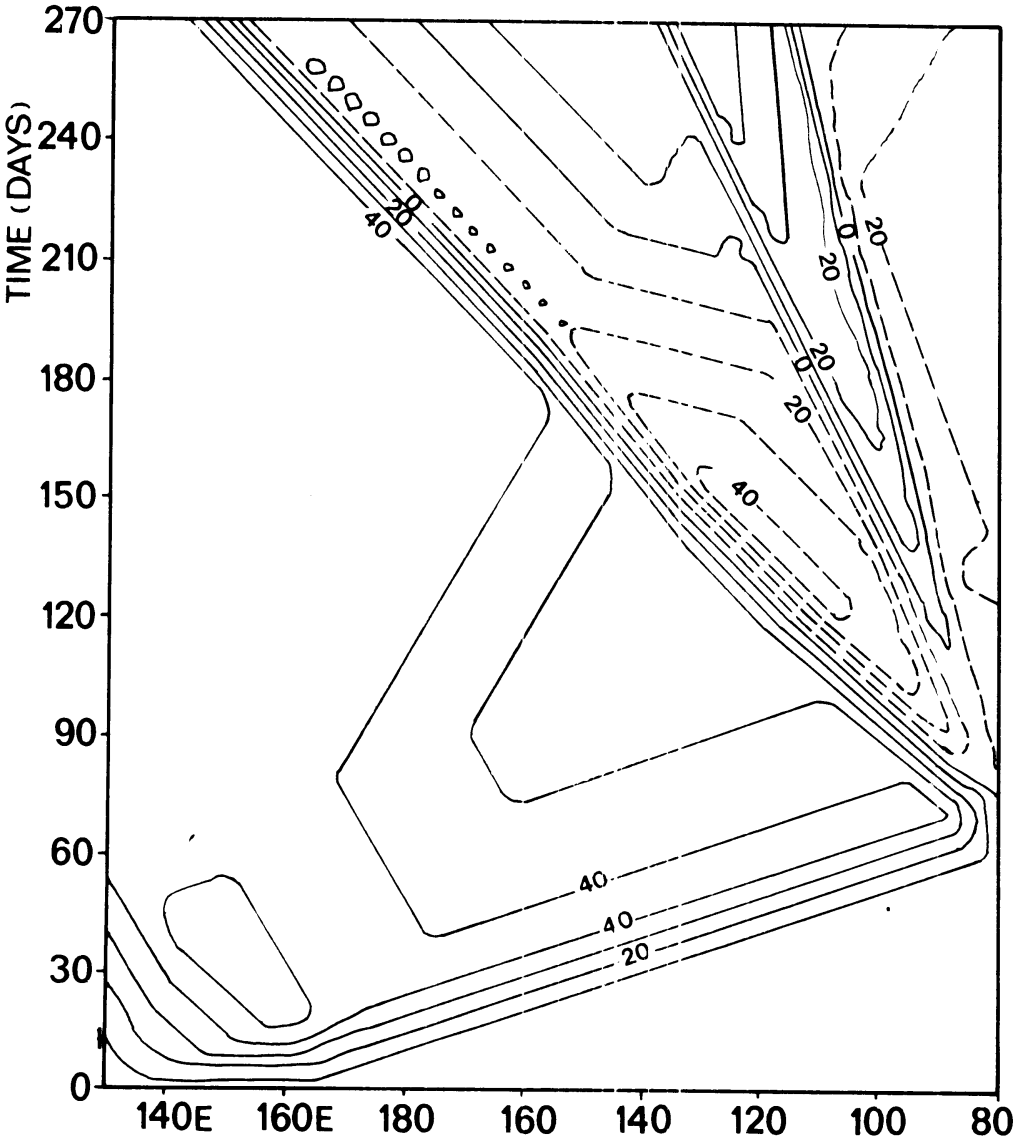
TIME (DAYS)
270
240
210
180
150
120
90
60
30
0
140E
160E
180
160
140
120
100
80
LONGITUDE (DEG)
40
20
20
20
20
40
40
40
20

figure 16 (b)

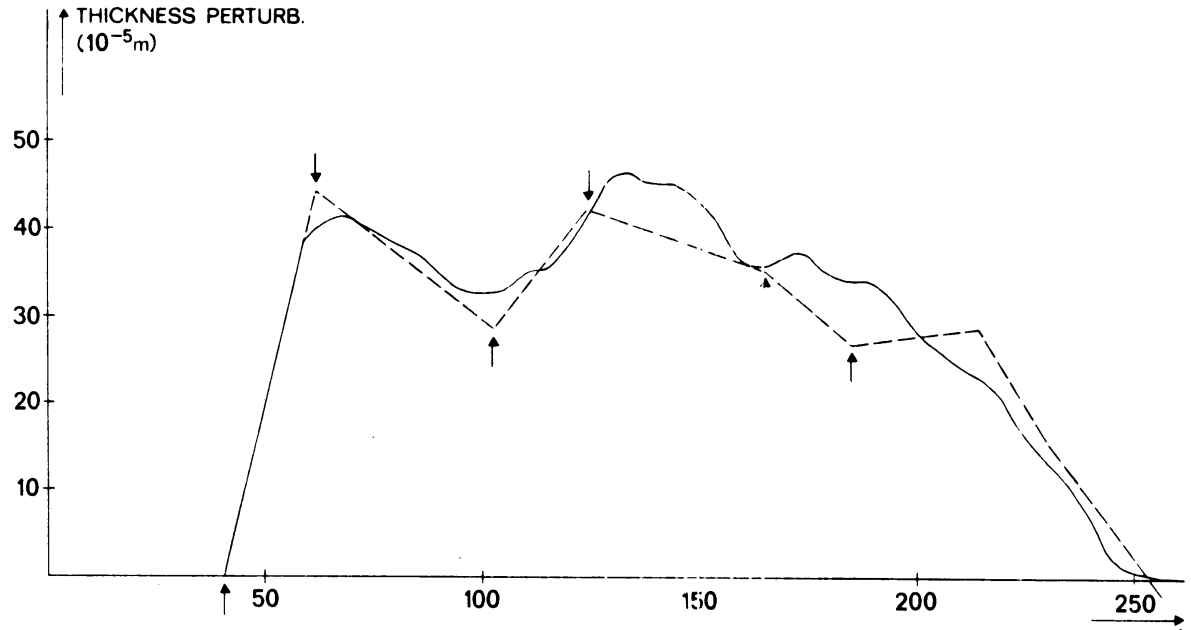


figure 17(a)

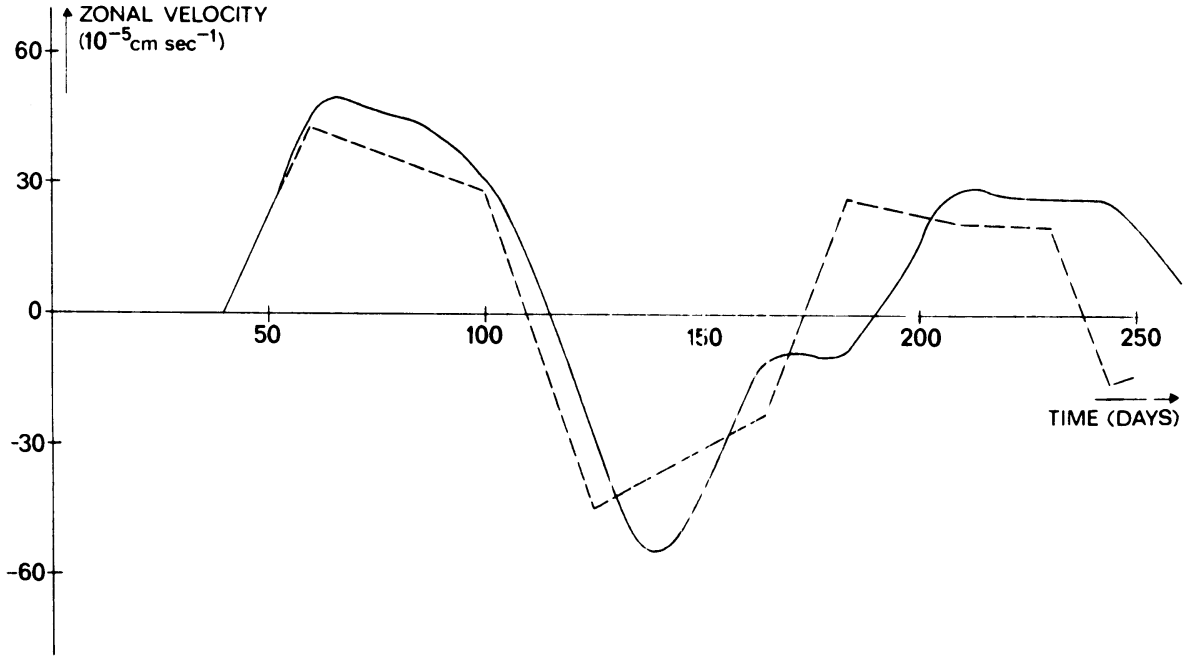


figure 17 (b)